Vedran Vuković

Test environment for X-ray photon detection in medical imaging

Master Thesis
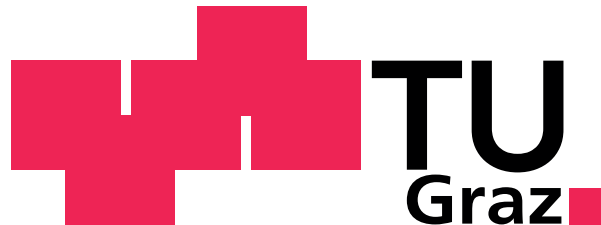
Institute of Medical Engineering

Technische Universität Graz

Kronesgasse 5, A - 8010 Graz

Head: Univ.-Prof.Dipl.-Ing.Dr.techn. Rudolf Stollberger

Institute of Electronics

Technische Universität Graz

Inffeldgasse 12/I, A - 8010 Graz

Head: Univ.-Prof.Dipl.-Ing.Dr.techn. Bernd Deutschmann

Academic advisor:

Dr. mgr inz. Alicja Malgorzata Michalowska-Forsyth

Evaluator:

Ao.Univ.-Prof. Dipl.-Ing. Dr.techn. Hermann Scharfetter

Graz, May 11, 2020

EIDESSTATTLICHE ERKLÄRUNG

Ich erkläre an Eides statt, dass ich die vorliegende Arbeit selbstständig verfasst, andere als die angegebenen Quellen/Hilfsmittel nicht benutzt und die den benutzten Quellen wörtlich und inhaltlich entnommene Stellen als solche kenntlich gemacht habe.

Graz, ...03.06.2020.........

(Datum)

....

(Unterschrift)

STATUTORY DECLARATION

I declare that I have authored this thesis independently, that I have not used other than the declared sources/resources, and that I have explicitly marked all material which has been quoted either literally or by content from the used sources.

Graz, ...03.06.2020.........

(date)

....

(signature)

Acknowledgement

Abstract

The aim of this master thesis was to develop a test environment for an X-ray photon detection. To accomplish this task, the current methods in medical imaging were ascertained, more specially the common detector and their processing. A wide-ranging research gave details about some signal specifications and further ideas for designing the circuit. The test environment included the controlled signal generation, which reproduces the impact of photons on the detector followed by a signal. Next up was to ensure, that the current signal is suitable for further processing, where a conversion into a voltage signal should be guaranteed. Additionally, the developed circuit was then tested on its signal generation property and was compared to another common method of short pulse generating, the Switched Capacitances. The pulse generation properties included the signal shape, the pulse width, the speed and the repeatability of the signal itself.

Kurzfassung

Das Ziel dieser Masterarbeit war eine Testumgebung für einen Photonendetektorsystem zu entwickeln. Dazu wurden die derzeitigen Methoden in der medizinischen Bildgebung ermittelt bzw. die gängigen Detektoren und deren Verarbeitung um sowohl die Spezifikationen als auch eine schaltungstechnische Lösung zu finden. Für die Testumgebung galt zunächst eine kontrollierte Erzeugung der Signale zu gewährleisten, die das Auftreffen der Photonen wiedergibt. Als nächstes sollte die Signalaufbereitung erfolgen, da es sich bei der Erzeugung um einen Stromimpuls handelt und ein kleiner Spannungsimpuls zum Auslesen benötigt wird. Des Weiteren wurde die entwickelte Platine auf ihre Signalerzeugungseigenschaften getestet. Außerdem wurde eine weitere Methode zur schnellen Pulserzeugung hinzugezogen und mit der Avalanche-Methode verglichen. Das Testen der Pulserzeugungseigenschaften beinhaltete die Signalform, die Pulsbreite, die Geschwindigkeit und die Wiederholbarkeit des Signals.

Executive Summary

The purpose of this thesis is to develop a testing environment for a Photon counting detector without using an X-ray source. These X-ray detection techniques are currently used in detection systems in medical imaging, since they deliver good image qualities. But they are very expensive in the everyday usage and more importantly they are harmful for the patient because of their ionizing radiation. From the point of view of electronics, the most important problem is that it is complicated and expensive to perform tests with a detector, so the electrical characterization, the proof that the circuit works, must be done before connecting the detector. The energy levels are adapted to the test environment, to illustrate the effect. Two pulse generation concepts were created: Avalanche and Switched Capacitance. The Avalanche circuit uses a bipolar transistor which triggers a short current pulse due to the Avalanche effect. For correct measuring, the current pulse must be transmitted to the Charge Sensitive Preamplifier (CSP). Put simply, it is an operational amplifier with a capacitance in the feedback loop. Therefore, the input current can be integrated proportional into an output voltage. These generated voltage pulses are then passing a threshold given by a comparator to preselect only the peaks of the pulses and afterwards counted by two 4-Bit binary counters.

The Switched Capacitance uses four fast-switching transistors and two capacitances to generate short pulses similar to the Avalanche pulses. The output pulse is also a current and therefore a CSP is needed to provide an equivalent voltage. Both pulse generators have surprisingly short pulse widths, but on the other hand the total charge was far away (10^{-9} Coulomb) from the desired 10^{-15} Coulomb range.

Table 1 – Comparison between Avalanche Pulse Generator and Switched Capacitance Pulse Generator

Avalanche Pulse Generator		Switched Capacitance Pulse Generator	
Frequency range	1 kHz - 70 kHz	Frequency range	Hz range - MHz range
Pulse width	24.8 ns	Pulse width	28.4 ns
Total charge	1.38 nC	Total charge	4.82 nC

Contents

Abbreviations

fC	femto-Coulomb
pC	pico-Coulomb
pF	pico-Farad
k	kilo
mV	milli-Volt
MHz	Mega-Hertz
THz	Tera-Hertz
ns	nano-second
CSP	Charge Sensitive Preamplifier
PcCT	Photon Counting Computer Tomography
PCD	Photon Counting Detector
SC	Switched Capacitance
EID	Energy-integrating Detectors
SNR	Signal-to-Noise-Ratio
ASIC	Application Specific Integrated Circuits
Photons/s	Photons per second
EMC	electromagnetic compatibility

List of symbols

Icon	Description	Important parameter
	Voltage supply	Voltage (Volt [V])
	Resistance	Resistance (Ohm [Ω])
	Capacitance	Capacitance (Farad [F]) Charge "Q" (Coulomb [C])
	Signal generator (rectangular or sinusoidal pulse with a specific on-time and off-time)	Voltage (Volt [V]) Time, Period (second [s])
	Bipolar transistor	Voltage (Volt [V]) Current (Ampere [A])
	MOSFET transistor	Voltage (Volt [V]) Current (Ampere [A]) Time (second [s])
SW1	Switch	On-Off Time (second [s])
	Operational Amplifier	Voltage (Volt [V]) Current (Ampere [A]) Time (second [s]) Frequency (Hertz [Hz])
	GND (Ground) reference point in an electrical circuit	direct physical connection to the earth (0 V, 0A)
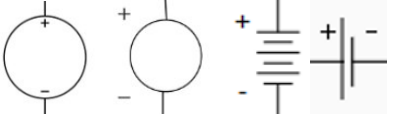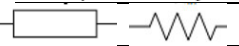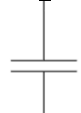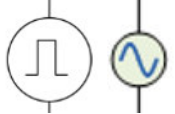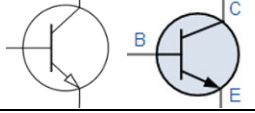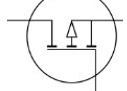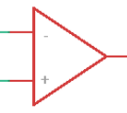
1 Introduction

1.1 Problem Statement

Detection systems in medical imaging have to be accurate and fast for the correct detection of X-rays in diagnostic techniques such as Positron Emission Tomography or the classical X-ray computer tomography. These detectors and their processing electronics should also be robust against signal disturbances from environmental impact. Advanced X-ray detection techniques like Photon-counting CT (PcCT) use Photon-counting detectors (PCDs) to detect individual single photons, which results in improved imaging quality. The main idea of this master thesis is to develop a testing environment for such a PCD without using an X-ray source. Therefore, the focus lays on testing the signal acquisition of a PCD by generating short pulses, which emulate incoming photons.

1.1.1 Goals

Controlled charge pulse generation - The most important goal for this thesis is to provide an accurate and reliable signal generation, which should emulate the photons generating a signal and their impact. Therefore, the design of the pulse generator should deal with following signal properties:

- Pulse width
- Pulse shape
- Pulse amplitude
- Pulse rate

In the first instance these signal properties must be determined by literature research. The next step is to develop an electrical circuit to generate short pulses. These pulses should correspond as closely as possible to the pulse shape and pulse duration from the literature research. The second goal deals with the readout of the pulses. An appropriate additional circuit is to be developed and fitted to the pulse generation circuit.

The last goal features the quantification of the generated pulses by counting each pulse for further evaluation.

1.2 Introduction into X-ray photon detection in medical imaging

1.2.1 Overview
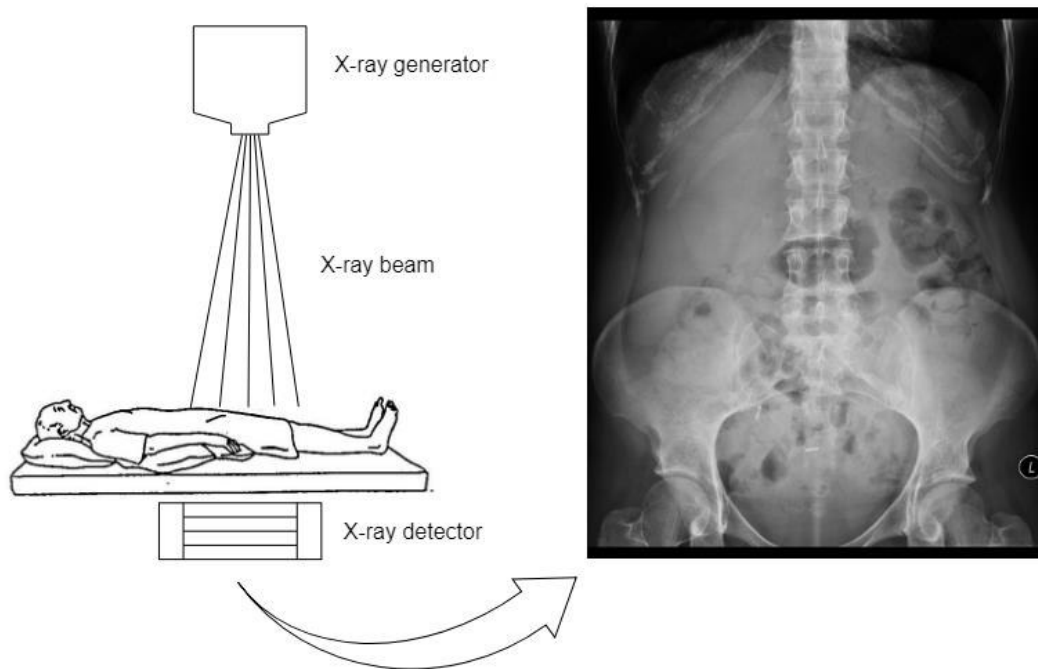
Figure 1 - Schematic of a standard X-ray system

source: (Yermie, 2019) (radiopaedia, 2019)

An X-ray system as often used in medical facilities consists of an X-ray generator, a rest table for the object or patient and an X-ray detector, which is located directly underneath. Figure 1 shows a simplified schematic of an X-ray system. There are further systems which have more components or different arrangements depending on the medical procedure.

The generator produces the X-rays and then directs them to the object to be observed. Within the tube a cathode is located, which is powered by a high voltage source applied between the filament and an anode. Thus, the tungsten filament of the cathode is heated up and emits electrons caused by the thermal electron emission. These emitted electrons are now accelerated and directed towards the anode on the other side of the tube. Due to the collision with the anodes surface X-ray quanta are radiated.

The interaction with the observed object is an important point for imaging. Basically, it is an attenuation of the X-ray photons due to the mass attenuation coefficient of e.g. a human body (bones, tissue, etc.). X-ray radiation can be absorbed and scattered. Both processes contribute to the mass attenuation coefficient.

After the observed object is passed, the remaining photons, which represent the attenuated flux, have to be detected by a detector system. This system can be either a simple system, as for example an X-ray film, or a complex system like a digital X-ray image acquisition system. For the simple X-ray film, the photons hit upon a so-called emulsion layer. This is followed by a chain reaction within the layer and a film development. The complex system consists of a converting layer and a matrix of several Charge-Coupled-Device chips (CCD) with additional control electronics. In the first place the photons are converted indirectly into visual light. Afterwards the visual light is detected by the matrix of CCD-chips. In both cases the detector has to convert the photons directly or indirectly for further processes to get the actual needed image. There are also possibilities to measure the spatial distribution, the spectrum or other X-ray properties.

A technique, that is based on the X-ray imaging, is the Computed Tomography (CT). With its fast scanning speed and high spatial resolution, it revolutionized the diagnostic medicine in the past decades.
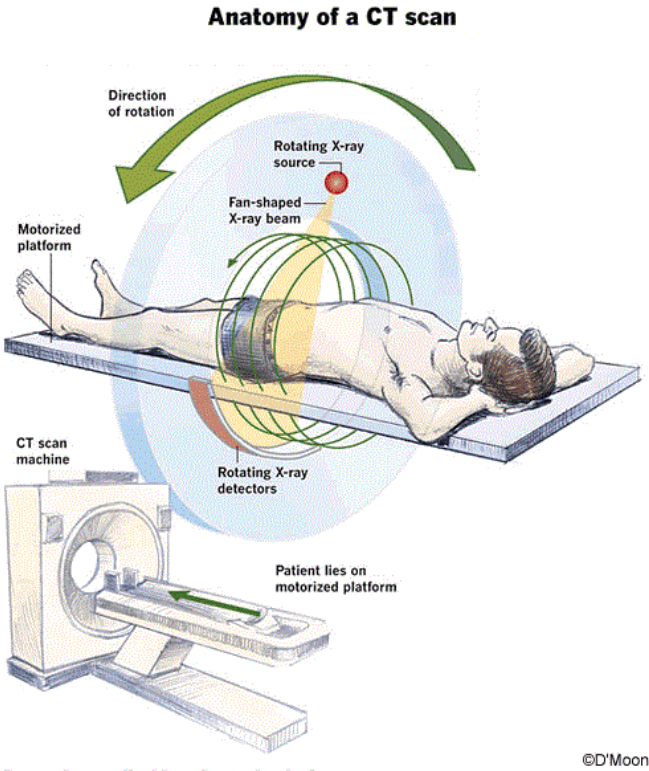
Figure 2- Schematic of a CT scanner

source: (Arizona Institute of Urology, 2019)

In Figure 2 one can see a schematic of a CT scanner. The most important part of a CT scanner is the detector ring. It affects the image quality as well as the radiation dose. Current scanners use solid state detectors and are constructed in 3rd generation rotating design. Over the years more special products were built on the basis of the CT and the Photon counting detectors (PCD). They have been introduced as an experimental part to the existing CT scanner. Due to their different physical mechanism in photon detection they are advantageous over conventional CT detectors.

1.2.2   Photon-counting Computed Tomography (PcCT)

PcCT is a specialized method for gathering more detailed information about the object to be observed due to photon counting. It has been developed and launched decades ago and since then it's been improved due to technical advances. Basically, PcCT uses Photon-counting detectors (PCD) and gathers far more information about e.g. tissues than conventional CT procedures due to their individual registration of photon interactions. This technique provides the possibility to distinguish multiple contrast agents. It has a good signal-to-noise-ratio and an improved spatial resolution compared to general techniques. Big challenges are the huge amount of data which is produced and the high counting rates. "Thus, the signal from PCDs carries with its energy information about each individually detected photon[1]".

1.3   Detectors used in Photon Counting

Photon Counting Detectors can discriminate individual X-ray photon energies. They differ from common energy-integrating detectors because of their working mode. PCDs work in pulse mode whereas common detectors work in current mode. Due to the pulse mode it is possible to process and register each photon individually. PCDs show many advantages such as high spatial resolution and low electronic noise (good SNR). They are also used for other imaging techniques like Positron Emission Tomography or Single Photon Emission Computed Tomography. Conventional energy-integrating detectors (EID) use the so-called indirect conversion method to provide detected X-ray quanta as an electrical signal. An EID consists of layers of scintillators, which convert X-ray photons into visible light and afterwards a photodiode detects the light and converts to an electrical charge in the following step. A reason why EIDs are not as good as PCD to count photons is their integration of the energy of all detected photons. The output signal does not carry any information of the energies of individual photons.

---

[1] (Katsuyuki Taguchi, 2013)

On the other hand, PCDs are based on the direct conversion method, where the semiconductor material converts the incoming X-ray photons directly to an electrical charge. In Figure 3 one can see the schematic of a semiconductor based PCD. Electron pairs are directly generated as X-ray photons arrive at the detector. The anode then collects all electrons, which are then released by applying a bias voltage throughout the semiconductor. The input photon energy is roughly equal to the output electrical signal. Therefore, each photon with a specific energy will generate a different electrical signal. Thus, each pixelated anode has two or more parallel channels. Each channel consists of a comparator and a counter. "Each detected signal is compared with a voltage that has been calibrated to reflect a specified photon energy level, referred to as an energy threshold.[2]" This energy thresholds can be seen in Figure 4. If the specific photon energy is in the range of the threshold, the counter increases its number of detected photons. Common PCD material is Cadmium-Telluride or Cadmium-Zinc-Telluride as well as germanium arsenide or silicon. (Shuai Leng, 2019)
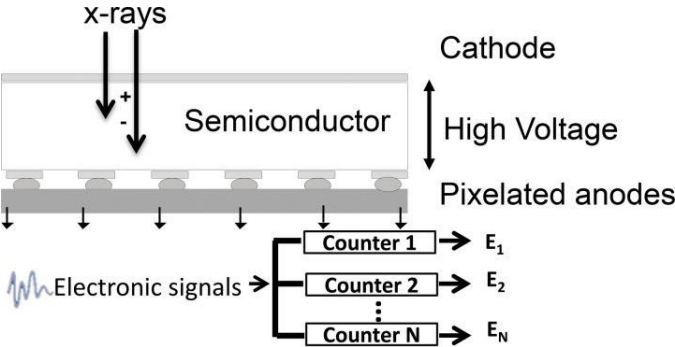
Figure 3 - Schematic of a PCD
source: (Shuai Leng, 2019)
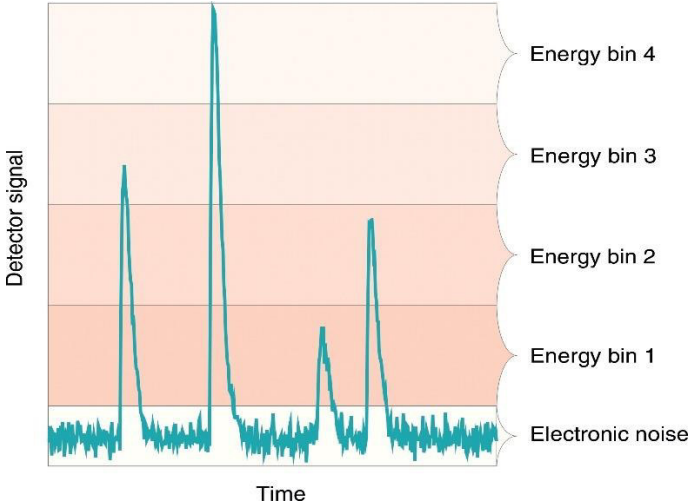
Figure 4 - Illustration of the operating principle of a PCD
source: (Martin J. Willemink, 2018)

---

[2] (Shuai Leng, 2019)

1.4   Overview of the detector components
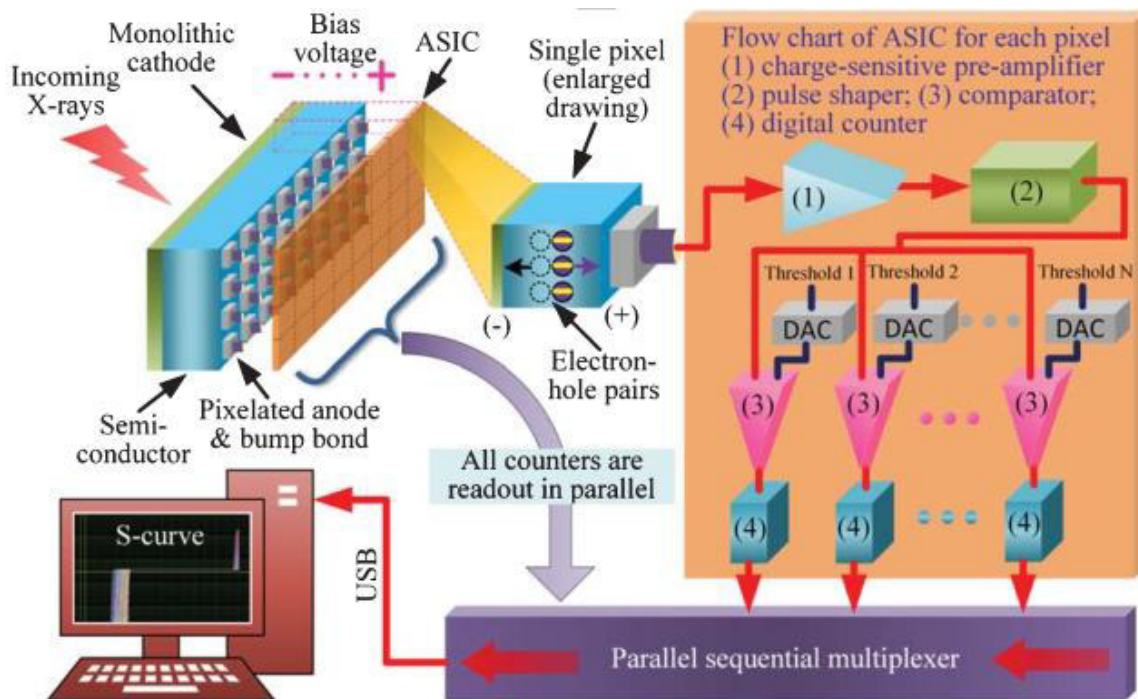
Figure 5 - Schematic of a semiconductor-based photon counting detector
source: (Liqiang Ren, 2017)

In general, a PCD can be split into two core parts: semiconductor material with two electrodes and application specific integrated circuits (ASICs) as shown in Figure 5. In the first part the semiconductor shares a monolithic cathode to receive X-ray photons. On the other side of the semiconductor pixelated electrodes are evenly distributed. These electrodes are connected to the ASIC through bump bonding processing. In this example 32 pixels are available and it can be extended through aligning multiple modules. Additionally, "a reverse bias voltage is applied between the two electrodes to create an external electrical field.[3]" The second part in Figure 5 is simplified for a single pixel and illustrates how an X-ray photon is detected, processed and registered. "When an incident X-ray photon interacts within the semiconductor material, electrical charges with an amount proportional to the deposited energy of the incident photon are produced and drift towards the monolithic and pixelated electrodes separately under the influence of the externally applied electrical field. During the drifting process of electron-hole pairs, a transient current is generated and then processed by the connected ASIC through one Charge Sensitive Preamplifier, one pulse shaper (shaping amplifier) and multiple pairs of voltage pulse height comparator and digital counter.[4]"

---

[3] (Liqiang Ren, 2017)
[4] (Liqiang Ren, 2017)
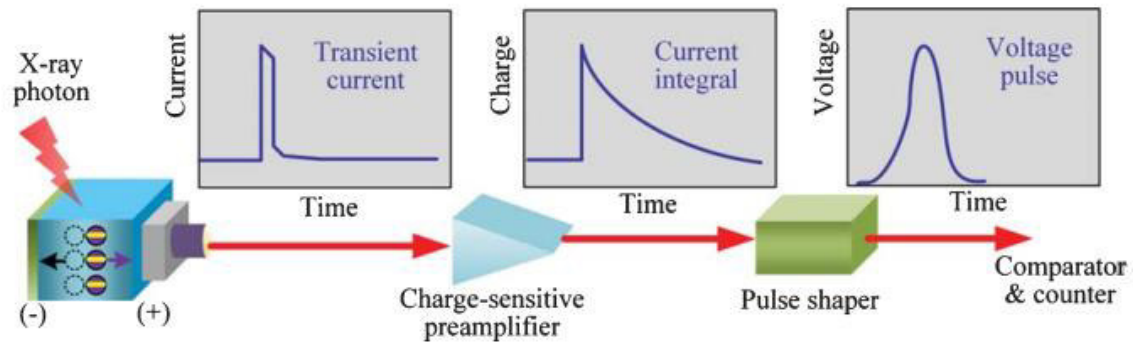
Figure 6 - Schematic of the second core part of a PCD
source: (Liqiang Ren, 2017)

The Charge Sensitive Preamplifier (CSP) measures the transient current through integrating by a feedback capacitor. As aforementioned, the deposited energy is proportional to the quantity of the generated charges within the semiconductor. The generated charge equals the transient current over time. "The output of the CSP is a voltage step proportional to the time integral of the input current pulse.[5]"

The pulse shaper or shaping amplifier shapes and amplifies the output voltage of the CSP. The additional amplification increases the signal intensities. But mainly the noise generated in the CSP is supressed to maximize detection accuracy. The purpose of a pulse shaper is to change the waveform of the transmitted signal due to a better suited for its communication channel (= physical transmission medium for example wire). This is achieved by limiting the effective bandwidth through filtering.

Lastly after the pulse shaping the signal is simultaneously sent to multiple comparators. Their purpose is to compensate the pixel-to-pixel variations caused by variations of electronics. This process is called threshold equalization. If the electrical signal has passed a certain threshold level the corresponding counter is triggered and a count is registered. (Liqiang Ren, 2017)

1.4.1 Signal characteristics

Before it has to be stated, for which purpose a signal generator is needed, several scientific articles were searched for specifications or recommendations for the signal properties for the input and the output of detectors in PcCT. Due to the different detector systems (APDs, CdZnTe semiconductor material) and the different application experiments (different processing electronics, number of channels and different amplifications) many different values for the pulse width as well as for the total charge were recommended or determined. Therefore, a broad range of recommended values of pulse

---

[5] (Liqiang Ren, 2017) – Charge Sensitive Preamplifier

width, total charge and counting rates were summarized at first to get a better overview on how to design the pulse generator.

Table 2 - Recommended signal properties[6]

Pulse width	Current signal before CSP
	> 20 ns
Total charge	fC - range
Charge Sensitive Preamplifier output	mV - range
Count rates	> 10^6 photons/s
Pulse shape	unipolar shape

Within the scope of this master thesis, a pulse generation technique, processing with a CSP and counting of pulses was developed. The pulse width was neither fixed to a certain value nor to the total charge. The setup concentrated on the realization of a ns-pulse generation as well as the count rate up to 10^6 pulses/s. If possible, the charge was kept in the pC - range.

---

[6] Summarized recommendations from (Huiming Zeng, 2013), (Liqiang Ren, 2017), (R. Ballabriga, 2016), (Shuai Leng, 2019) and (C.G. Jakobson, 1999)

2 Methods

2.1 Pulse generation concept

Due to the recommended signal properties as listed in Table 2, two possible pulse generator circuits fulfil the requirements. The first circuit is based on a familiar physical effect, the so-called Avalanche Effect. This circuit offers short pulsing in the nanosecond range depending on the characteristics of the chosen transistor as well as the chosen capacitance C_S, see Figure 15. On the other hand, this effect has a stochastic behaviour, which constrains the pulse rate adjustment. Therefore, the second - the Switched Capacitance - serves as a backup for comparison and the possibility to adjust the pulse rate. First, both circuits along with their components will be explained and afterwards they will be compared to one another. As for the result section the main focus will stay on the Avalanche Pulse Generator due to its interesting Avalanche effect as well as fact that this physical phenomenon is not commonly used in the state-of-the-art electronics.
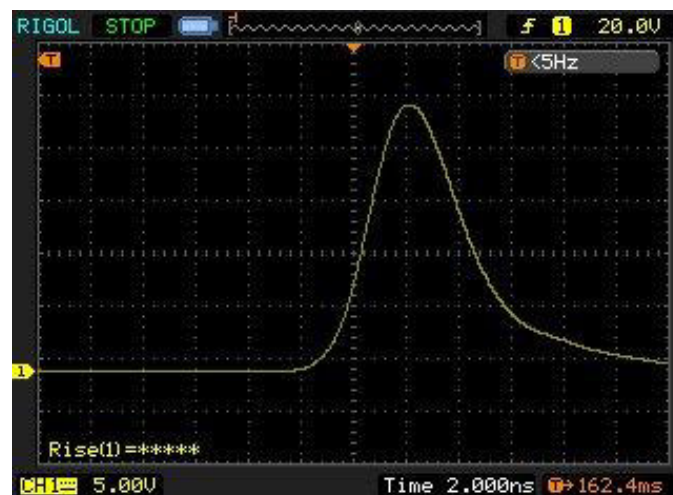
Figure 7 - Avalanche Pulse signal as shown on the website of (Wong, 2019)

Some scientific websites (including (Wong, 2019) a website created by Kerry D. Wong, graduate from the University of Wisconsin – Madison) explained how simple and effective such Avalanche Effect circuits can be. In Figure 7 one can see such an Avalanche pulse which was measured with an oscilloscope. It was presented on the website of (Wong, 2019).

2.2   Avalanche Effect

The so-called Avalanche Effect or Avalanche Multiplication is one of three breakdown mechanisms in junction breakdown of semiconductors. In general, a high electrical high field must be applied at first to a p-n-junction of a semiconductor to trigger this effect. If this electrical high field is greatly increased, the junction will break down at some specific voltage value and the transistor will conduct a large current as a result. For better understanding of the Avalanche effect, the junction of a diode will be explained in detail. (Sze & Ng, 2007)

2.2.1   P-N Junction

The junction can be described as a two-terminal device. It can have various terminal functions, which depend on the doping profile, device geometry and biasing condition. Each of the terminals is either a p-type doped or n-type doped semiconductor crystal.

- Zero-biased:

  If no voltage is applied at all, the charge carriers recombine in the region between both terminals (step 1 in Figure 8), more precisely directly at the boundary. A region is formed, which is called depletion zone (step 2 in Figure 8). A positive charge forms upon electron absence in the n-crystal region and a negative charge forms due to the diffused holes in the p-crystal region. At a specific level of this potential gradient, the re-combination of holes and electrons comes to a standstill and the charge carriers can no longer overcome the electric field.
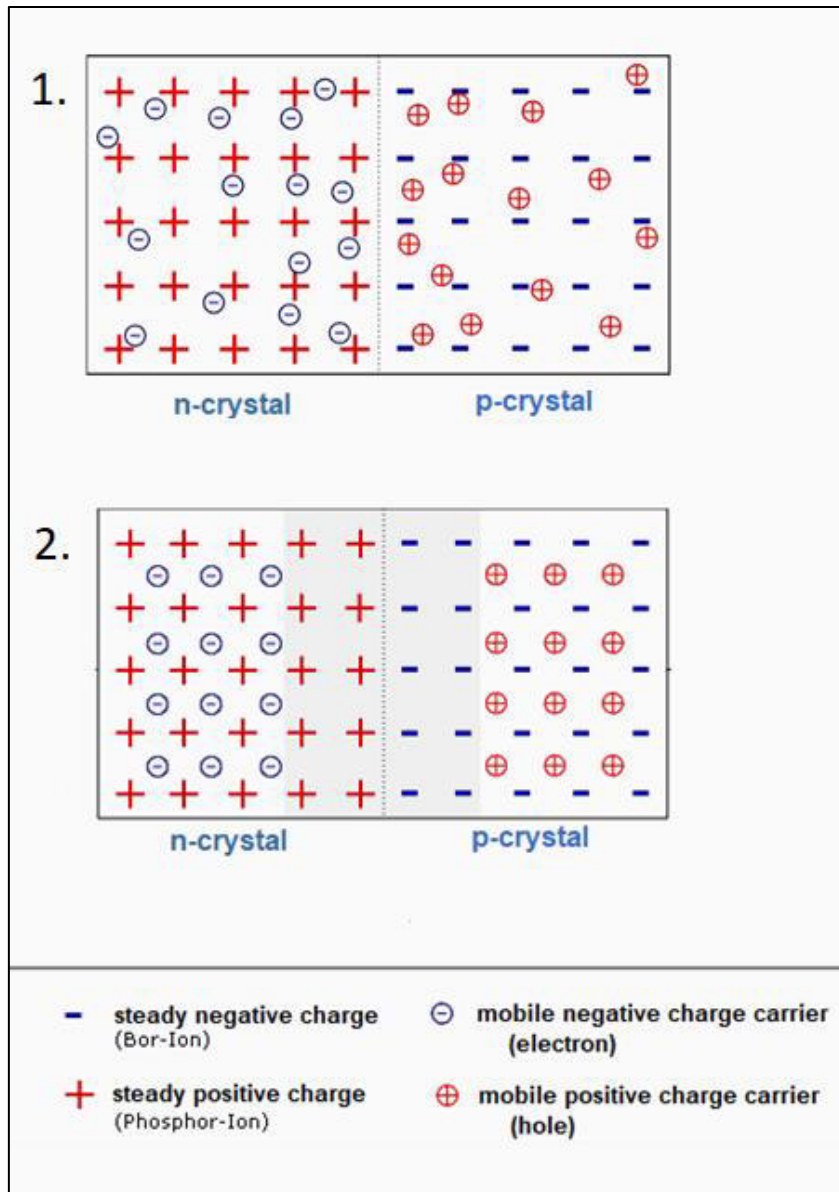
Figure 8 – No bias - step 1: Recombination starting and step 2: Depletion zone creation (dark grey coloured) source: (Laube, 2019)

- Reverse-biased:

  If a positive voltage is applied at the n-crystal and a negative voltage is applied at the p-crystal, both electrical fields (inner electrical field and external applied field) are aligned in the same direction. The inner electrical field is therefore amplified. As a result, the depletion layer enlarges and no current flow is possible. The free charge carriers are attracted to the poles of the external voltage source (Figure 9). (Laube, 2019)
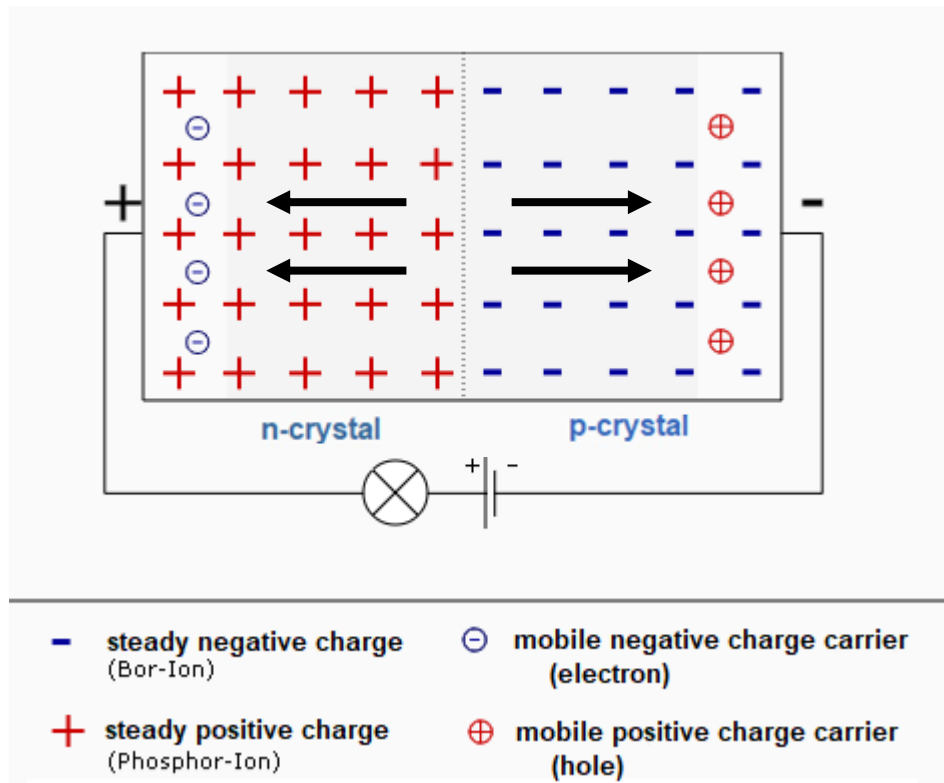
Figure 9 - Reverse-biased – Enlargement of depletion layer
source: (Laube, 2019)

- Forward-biased:

  The process is now repeated with swapped external voltages. The negative voltage is now applied at the n-crystal terminal and the positive voltage is applied at the p-crystal terminal. Now charge carriers are replenished continuously, which can recombine at the boundary. The depletion layer shrinks and the internal electric field can be overcome (Figure 10). As a result, a current is flowing.
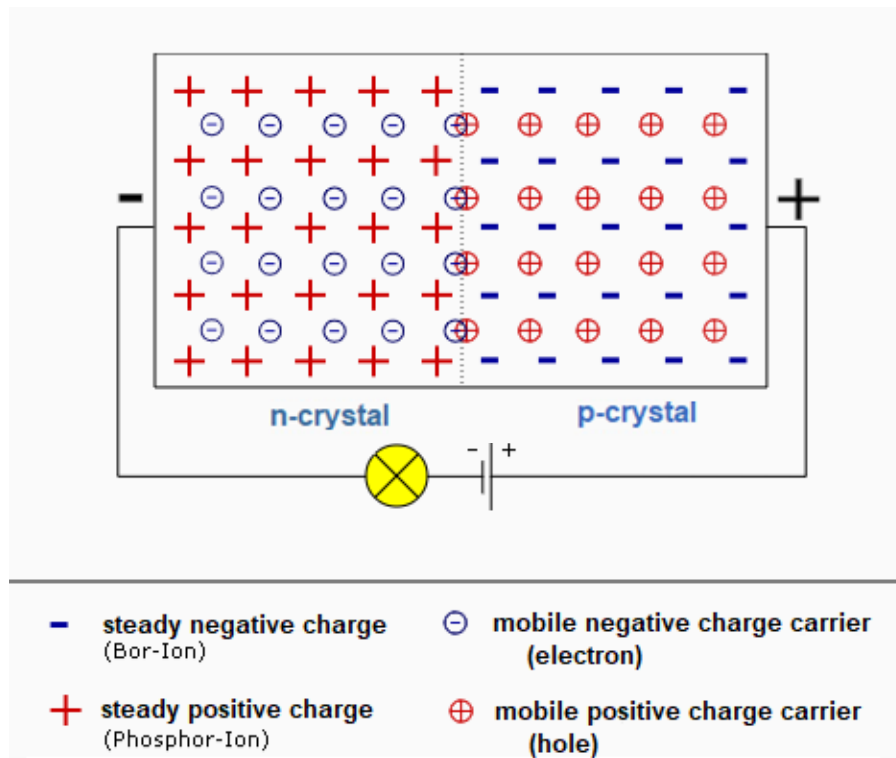
Figure 10 - Forward biased – current flow
source: (Laube, 2019)

2.2.2 Multiplication processes

Assuming that the junction or semiconductor is reverse-biased, the applied voltage will now be increased gradually. In reverse-biased free charge carries will be attracted to the poles of the applied voltage. These free charge carriers will be accelerated as more voltage is applied. At some point the accelerated electron has enough kinetic energy to hit another electron out of its bound state into the conduction band after colliding with the respective lattice atom (Impact ionization). As a result, the two electrons are moving freely. As more electrons are freed, more electrons can collide and hit up more electrons out of their bound state with their atoms. This turns into an avalanche effect and the value of current becomes incredibly high. Additionally, the breakdown process happens on extremely short timescales. (Whittemore, 2019)

Forward Current, I_F

Forward Characteristics

Reverse Voltage, V_R

Forward Voltage, V_F

Avalanche Breakdown Voltage, V_{BR}

Reverse Characteristics

Reverse Current, I_R

Avalanche Breakdown Curve
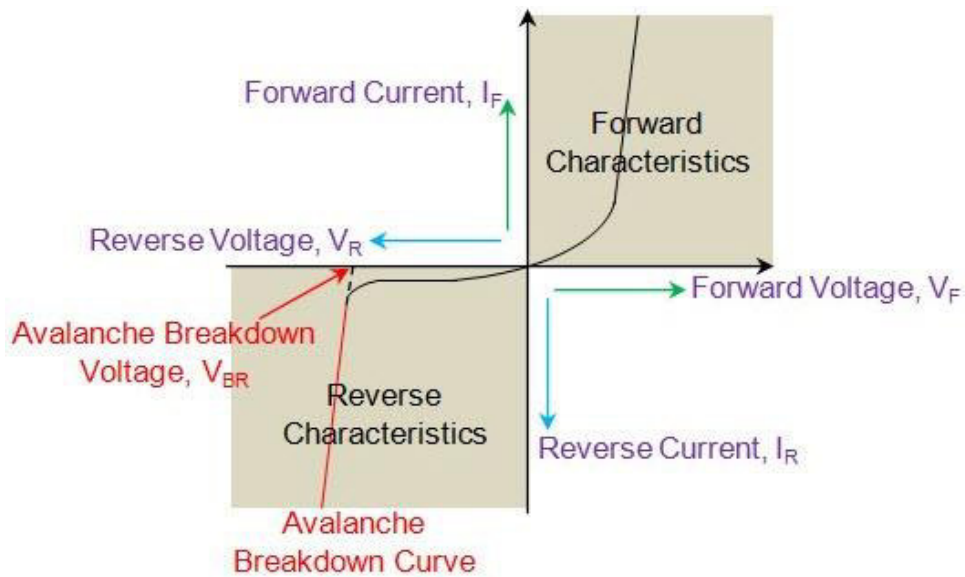
I-V Curve for a P-N Junction Depicting Avalanche Breakdown Phenomenon

Figure 11 - Diode characteristics curve - breakdown voltage
source: (Elprocus, 2020)

"Breakdown voltage is a parameter of a diode that defines the largest reverse voltage that can be applied without causing an exponential increase in the leakage current in the diode[7]", see (Figure 11). It ought to be considered, that the semiconductor should not be permanently run above the breakdown voltage. The semiconductor could be permanently damaged due to overheating owing to the non-stop accelerated and increased number of charge carriers. (learningaboutelectronics, 2019)

2.2.3 Transistor in general

A transistor junction consists of two individual p-n-junctions put back to back in series. This results in three layers, which share a common p- or n-terminal. A transistor can act as a conductor or as an insulator, which means that there are two main abilities: switching and amplification. Furthermore, there are two types to mention: NPN and PNP (see Figure 12). The difference between those types is the physical alignment of the p- and n-junctions. Three layers give the opportunity to connect three terminals: Emitter (E), Collector (C) and Base (B). It is possible to control large collector currents with a small current flowing into the base terminal. (Aspencore, 2019)

---

[7] (Meek & Craggs, 1978)
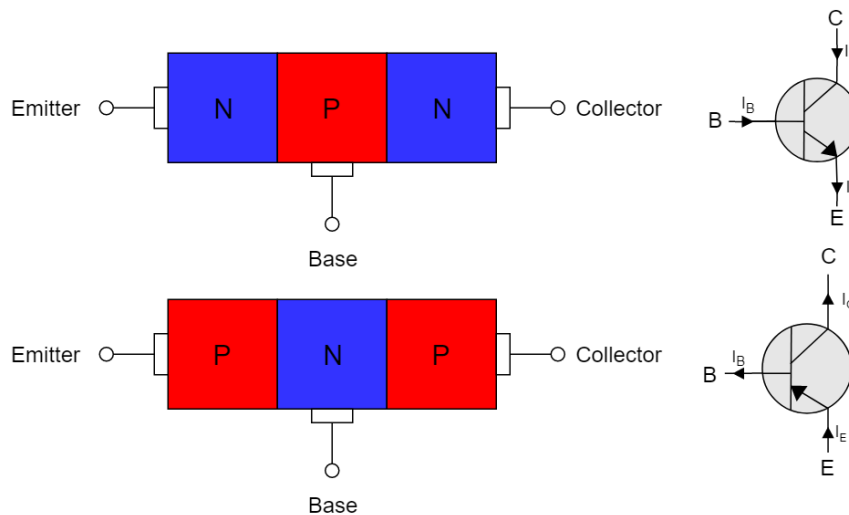
Figure 12 - NPN/PNP - Physical Appearance and Symbols

Basically, with three terminals there are three possible transistor configurations.

- Common Base configuration
- Common Emitter configuration
- Common Collector configuration

The Common Collector configuration will be discussed in detail, because the main pulse generation circuit is designed after this configuration. The other two will only be mentioned and not further discussed. (Aspencore, 2019)

2.2.4 Common Collector configuration for pulse generation

This configuration is meant for high current and low voltage gains. The collector is directly connected to the voltage supply. The emitter is connected with a resistance load in series to the ground so that the emitter current is equal to the load current, whilst the output is taken directly from the emitter load. The input signal is connected to the base. The following figure shows the configuration. (Aspencore, 2019)
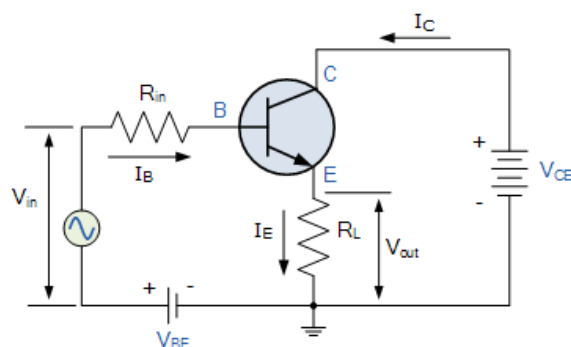
Figure 13- Common Collector Configuration
source: (Aspencore, 2019)

2.3 Design of testing environment

For simplification the whole circuit can be segmented into three functional parts (underlined in red). The first part is the pulse generator, which generates short pulses with adjustable pulse-rate and amplitude. The Attenuator is an additional part and is added due to the high current of the pulse generator. The Charge Sensitive Preamplifier is needed to convert the current pulse into an equivalent voltage step. This is followed by a comparator which compares the incoming signal with its reference signal. If the input signal is greater than the reference signal, the comparator generates a high signal at the output. If the opposite occurs, it generates a low signal.
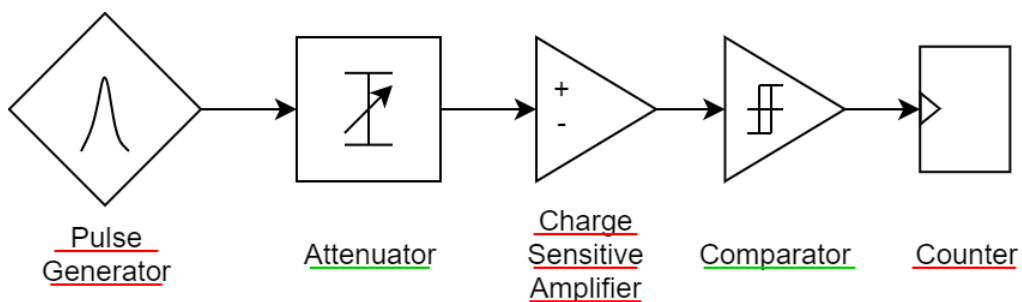
Figure 14 - Schematic of all functional parts

2.3.1 Avalanche Pulse Generator

2.3.1.1 Overview and Function

A transistor circuit is used to generate short pulses in combination with a capacitance for pulse width configuration. In the following figures, you can see the implemented pulse generation circuit.
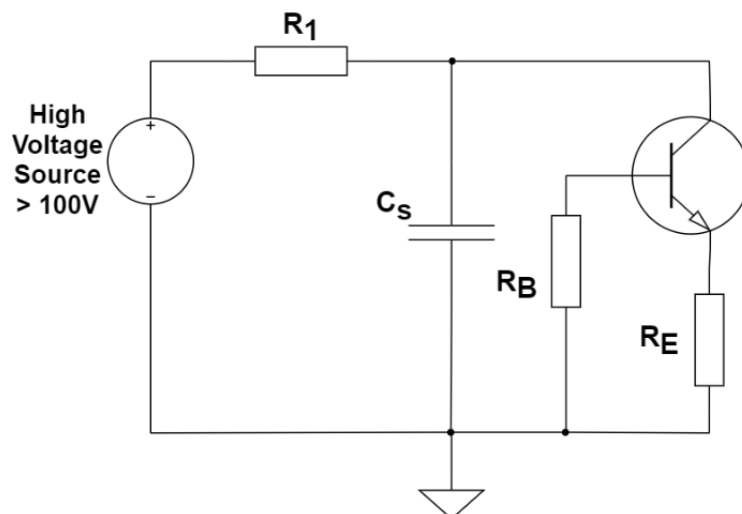
Figure 15 - Avalanche Pulse Generator

The Avalanche breakdown voltage is specific for each transistor model (e.g. with different Collector-Emitter-Capacitance and different Breakdown voltages) and it also differs between manufacturers and types. In the first attempts the voltage was increased stepwise until the breakdown took place. According to (Engdahl, 2019) and (Wong, 2019) the Avalanche voltage is reached at approximately 100 V to 120 V. A high current could be measured, which flows through the 50-Ohm emitter resistor R_E. The transistor must be protected due to the continuously flowing current and thus overheating and breaking of the junction. This is accomplished by a 220 k-Ohm resistance R_1. Secondly the capacitance of 10 pF C_S holds all the charge necessary for the momentary current. "Once the avalanching transistor has drained the capacitor, the collector is then at a low voltage and avalanche current stops. This gives the C_S capacitor a chance to recharge and the cycle begins again the next time the transistor avalanches. The 10k-Ohm base resistor R_B to ground is to ensure that the transistor stays off with the exception of avalanche operation[8]."

2.3.1.2 Pulse rate and Amplitude adjustment

In consequence of the stochastic behaviour of the Avalanche effect, the request to adjust frequency and amplitude could not be satisfied perfectly with the original version. The idea of triggering the Avalanche manually with an external pulse source was suggested during the project, which is represented in Version 2, see Figure 16. An important consideration was to apply enough voltage to reach nearly the Avalanche breakdown voltage, which was about 105 V for the modified version. With the help of the external pulse supply the Avalanche breakdown region could be reached. The additional rectangular voltage step was precisely set to 2V to trigger the avalanche at the rising edge. The modification is done by replacing the base resistor with the voltage pulse supply.
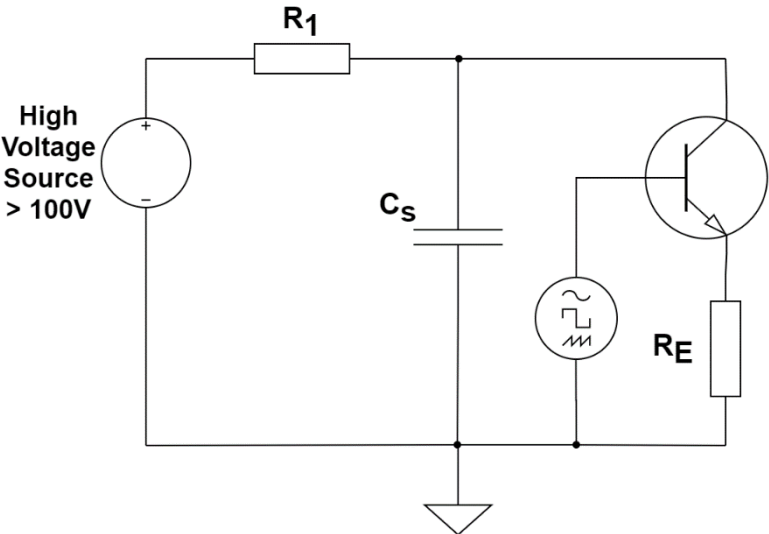
Figure 16 - Modified pulse generator - additional external pulse supply

---

[8] (Whittemore, 2019)

2.3.1.3   Attenuation

Due to the high output pulse amplitude, an attenuator was required for amplitude adjustment, in order to subsequently work with the other components, such as the operational amplifier and the comparator. The reasons for the attenuation are the maximum input signal levels of the operational amplifier and the comparator. Both components are supplied with 5V, which approximately determines their maximum input signal level up to 5V. The output signal of the avalanche pulse generator exceeds this set signal input level. The required picofarad charging range was also not met as mentioned in 1.4.1.

A simple solution is to decrease the generated current through a current divider. The purpose of a current divider is to divide the incoming current according to the wiring. The greatest current applies here at the branch or path of least resistance. This following equation describes the simple division of the current into a specific branch of interest.

$$I_X = \frac{R_T}{R_X + R_T} I_T$$
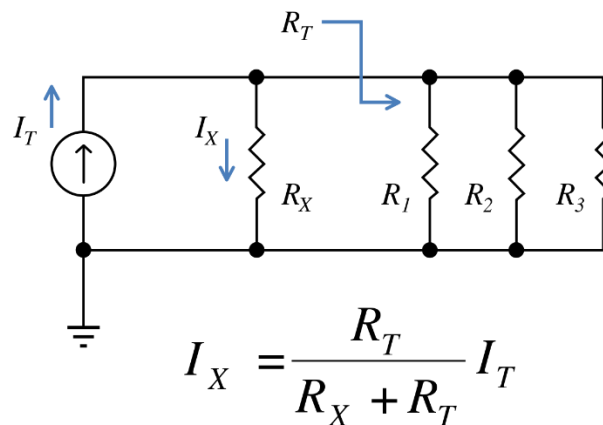
Figure 17 - Current divider
source: (Wikipedia, 2019)

In Figure 17 I_T is the total current. R_T represents the calculated total resistance of the combination of parallel resistors R_1, R_2 and R_3. R_T is calculated with the following formula:

$$R_T = \frac{1}{\frac{1}{R_1} + \frac{1}{R_2} + \frac{1}{R_3}} \tag{1}$$

This idea can be extended to a so-called T-pad, which is also a resistance network but particularly for signal attenuation with impedance adjustment for signals in the radio-frequency (RF). The RF-range ranges from 9kHz to THz as defined by the EMC-standard. (Wikipedia, 2019)
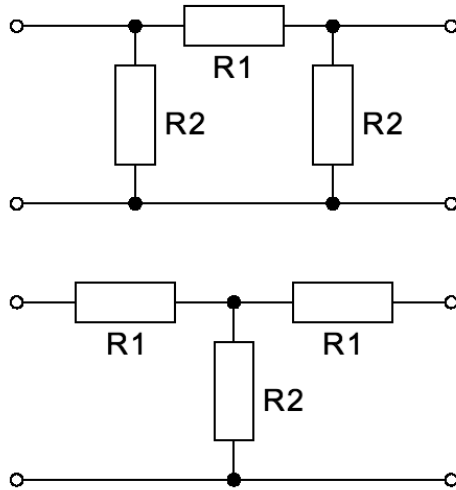
Figure 18 – T-Pad symmetrical/unsymmetrical
source: (Wikipedia, 2019)

The decision was made to use an external attenuator, as it was already available at the institute and immediately available. The chosen attenuator had an incremental attenuation in decibel steps. For the external circuitry two SMA connector jacks and SMA-to-N-jack adapters were required to connect the external attenuator.

Figure 19 - External attenuator with step adjustment
source: (Picclick, 2020)

For the selection of the transistor a few component properties must be considered before putting it into operation:

1. The breakdown voltage V_{CEO} defines the maximum applicable reverse voltage for the Collector-Emitter terminals. Above this voltage, the breakdown region is located and at some specific voltage level the Avalanche effect is triggered. The higher this voltage is stated in the data sheet (component specified), the more voltage must be applied with an external high voltage.

2. A second consideration should be the capacitance of the junction C_{CB} Collector-Base. It is assumed that this should be as small as possible. According to this assumption the capacity should not have a big influence on the pulse length. This could be proven by testing some transistors with different collector-base capacitances. This capacitance and also the other capacitance on the other terminals (Collector-Emitter and Base-Emitter) are parasitic due to the terminals of the transistor, which are made of conducting material. "At higher frequencies these capacitances can affect amplifier performance[9]." Additionally, these capacitances also have an influence on the junction cross-section. The smaller the capacitance and the smaller the diode, consequently the Avalanche current can be expected to be smaller as well. For further information and results on the influence of the capacitance, see Results chapter.

3. Some transistors are specialized as Avalanche transistors, which are constructed for such applied high voltages and high currents. If the transistor is labelled as such one, a peak collector current is also listed in the datasheet. It describes the maximum current flow, if an Avalanche is triggered. In some cases, the pulse width is also stated.

After testing some transistors including Avalanche transistors and some standard NPN transistors, the 2N3904 and the SMD version MMBT3904 NPN transistor were chosen. Several sources (Wong, 2019), (Engdahl, 2019) and (Whittemore, 2019) recommend this transistor due to its short pulse generation and low price. The Avalanche voltage is about 120 V if triggered without an external trigger source and about 105 V with an external trigger source. For both values the maximum signal amplitude is reached. For a more detailed illustration of the tested transistors, their junction capacitance and the breakdown voltage, a table was created in chapter 3.1.6 (Table 6).

---

[9] (Wong, 2019)

2.3.2 Switched Capacitance (SC)

As an alternative a second circuit was designed in parallel during the master project for comparison and as a back-up, if the avalanche circuit would not have been able to fulfil all expectations. The common switched capacitance circuit is used to test if short pulses in the range of 30 ns are possible to generate as well as to examine what total charge is possible to get. In the following figure a common switched capacitance is illustrated.
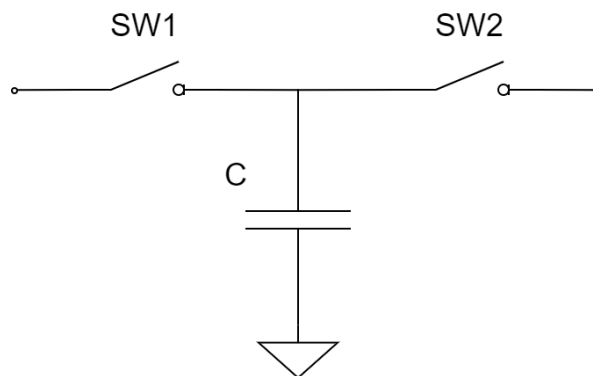
Figure 20 - Switched capacitance in general

2.3.2.1 Working principle of SC

In the following steps, the working principle of the SC is explained, with reference to Figure 20.

1) Initially SW1 is closed, while SW2 remains open. Capacitor C is either fully charged or only partially charged, because it is possible to determine how long the switch (SW1) remains closed. This restriction influences the total charge of the capacitor. Additionally, the total charge can also be increased or decreased by the connected voltage source (Figure 21).

2) Afterwards SW1 is opened and SW2 is closed. The charge taken up is emitted in the form of a current, which in turn is additionally regulated by the duration of the closing (SW2). Both switches as well as the capacitor C thus influence the output signal. The process can now be repeated as often as required and several pulses can be generated.

In this project, the focus is on the fast toggling of the switches as well as the choice of capacity value to ensure a short pulse width and a low charge per pulse. By adding an identical SC circuit, the number of pulses would also have a positive effect on increasing the pulse frequency. The following circuit (Figure 21) has been designed to meet those requirements.
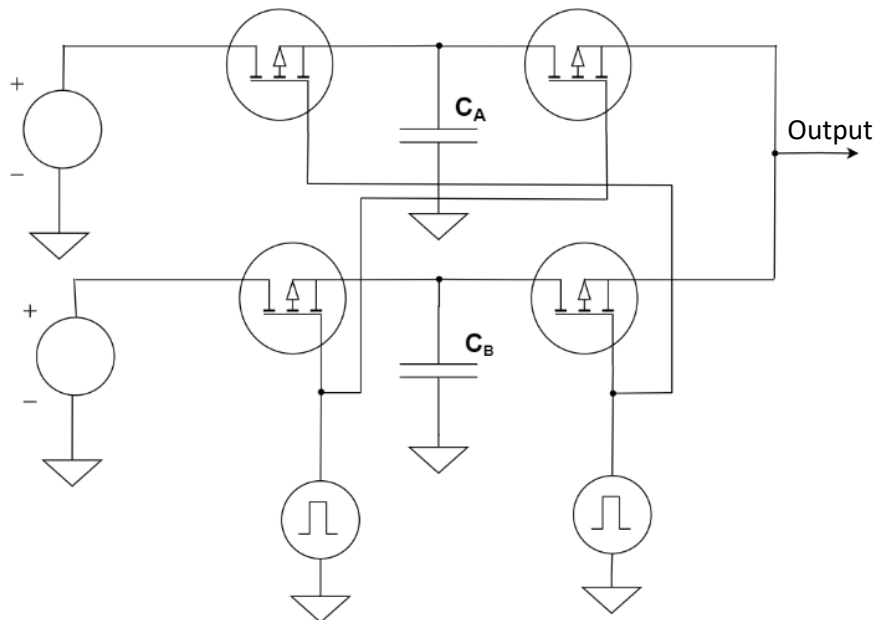
Figure 21 - Modified Switched Capacitance circuit for short pulsing

An important requirement for the correct choice of the switch was that it should be fast enough to guarantee a high pulse rate. A P-channel DMOS transistor was chosen because of its high-speed switching. The turn on time is 3 nanoseconds and the turn off time 7 nanoseconds. Furthermore, the parasitic capacitances of the transistor are in the pico-farad range. The pulse width to be generated is in the range of about 25 nanoseconds, so its switching times meet the requirements. With regard to the parasitic capacitances, these should be as low as possible, since they have an influence on the switching properties of the transistor. As an example, the output capacitance (C_{oss}) is mentioned, which is composed of the drain-source capacitance and the gate-drain capacitance. "If the output capacitance is large, a current arising due to C_{oss} flows at the output even when the gate is turned off, and time is required for the output to turn off completely."[10]

---

[10] (ROHM Co., Techweb, 2020)

Two additional pulse sources were needed for the switching of the transistors. Two function generators were used for the pulse sources. Both have the same amplitude of 1VPP and the same duty-cycle. Only with one function generator an additional delay-time was set to avoid overlapping with the signals of the other function generator. This ensures a correct turn-on and turn-off cycle for charging the capacitors. Only then is a doubling of the pulse frequency guaranteed. Furthermore, two pulse amplitudes can be achieved. The capacitance as well as the voltage must be matched to each other to ensure optimal charging for a good pulse shape. If the chosen voltage is too small, the capacitance cannot be charged optimal to produce the desirable amplitude. On the other hand, the amplitude of the output pulse would also be much higher than the desired charge. This thought experiment can also be repeated with the capacitance. Furthermore, the charging has to be additionally matched onto the switching time of the transistor. By testing different capacitances and adjusting the charge sources simultaneously, a satisfying pulse generation could be accomplished as shown in the Results section.

2.3.3   Charge Sensitive Preamplifier (CSP)

For further processing of the current pulse an equivalent voltage pulse is required. This can be implemented with a simple operational amplifier circuit. This is known as the Charge Sensitive Preamplifier. The design rules for the CSP include measuring the current pulse and the optimal output voltage step for further processing with the comparator and the counters. As a mentioned in 1.4, the input current pulse is proportional to the negative voltage step on the output due to integration with the feedback capacitance **C** (Figure 22).

2.3.3.1   *Overview and Function*
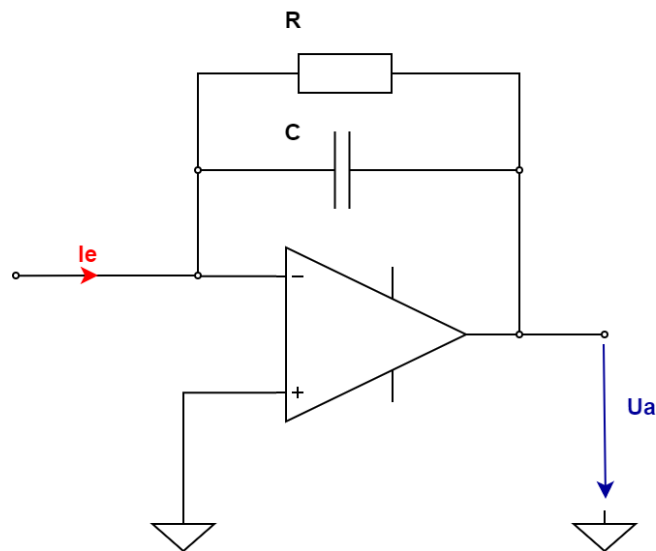
Figure 22 - Charge Sensitive Preamplifier in general

The following mathematical formula describes the relation between the voltage step (inverted) and the time integral of the current input pulse:

$$Q = C \cdot U \ \rightarrow U = \frac{Q}{C} \tag{2}$$

$$Q(t) = \int_0^t i(t) \, d\tau \ \rightarrow U(t) = -\frac{1}{C} \cdot \int_0^t i(t) \, d\tau \tag{3}$$

Essentially, the CSP consists of a capacitance and an operational amplifier (Op-Amp). It is based on a basic structure of the operational amplifier circuit: the integrator. The difference between a common integrator and a CSP is the resistance at the negative input of the operational amplifier. A resistor is required at the input when a voltage signal is present. In this case it is a current signal. Therefore, no

resistor is needed. To react to subsequent pulses, a resistor is placed in parallel with the capacitance in the feedback path. This has the effect of shortening the fall time (Figure 24). (physicsopenlab, 2019)

In the following pictures you can see the input and output signal of the CSP. It should illustrate how the CSP works. Figure 23 shows the input signal. This is a current pulse in the nanosecond range. The next figure (Figure 24) shows the output signal, a voltage step that inverts the signal due to the integrator. This results in a negative signal at the output. The signal is also shown in the nanosecond range. In the last picture (Figure 25) we are in the microsecond range, so that the whole pulse is shown.
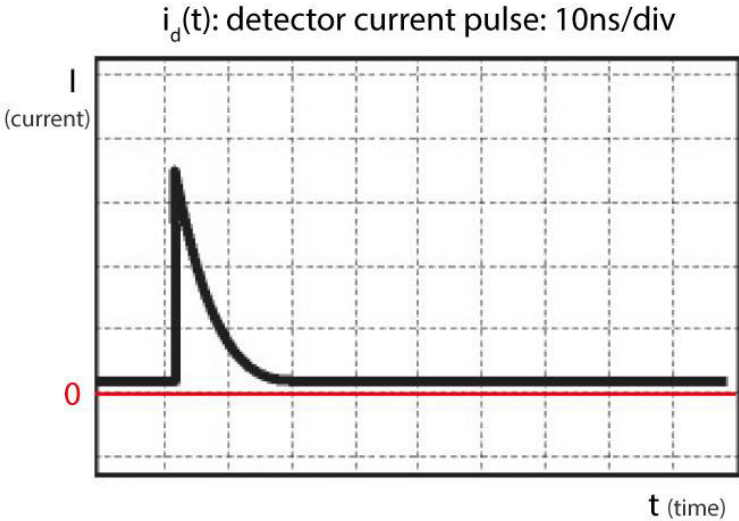
Figure 23 - Current input pulse with 10 ns/div
source: (physicsopenlab, 2019)
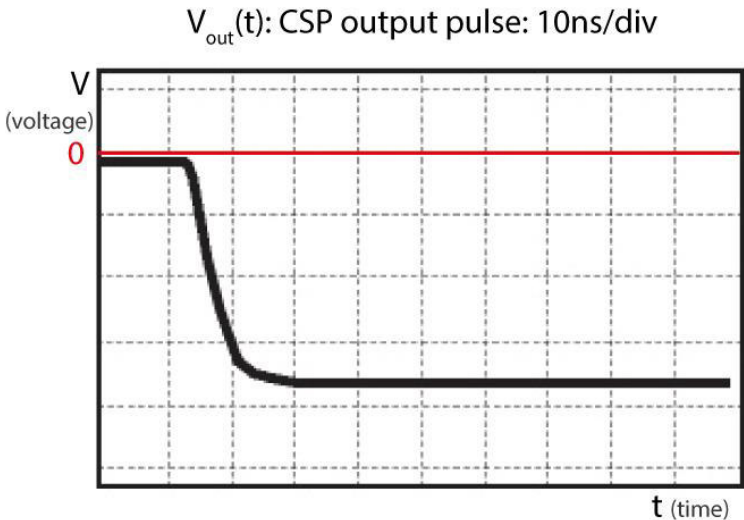
Figure 24 - Voltage output pulse with 10 ns/div
source: (physicsopenlab, 2019)
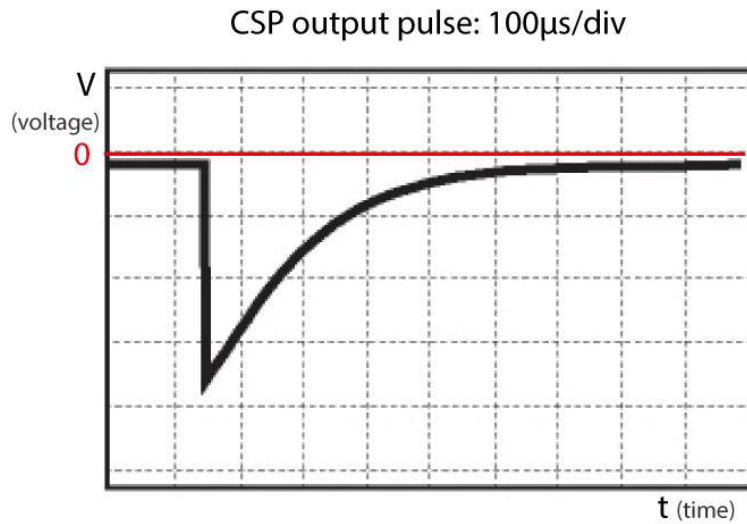
Figure 25 - Voltage output pulse with 100 μs/div

source: (physicsopenlab, 2019)

Due to the limited measurability with oscilloscopes one cannot simply measure the current pulse directly. By determining the rise time of the output voltage pulse, the pulse width of the current pulse can be measured indirectly. This is accomplished by setting the edges for the rise time at 10 % of the absolute pulse bottom and at 90 % of the absolute pulse top without considering possible over- or undershooting (Figure 26). (Mietke, 2019)
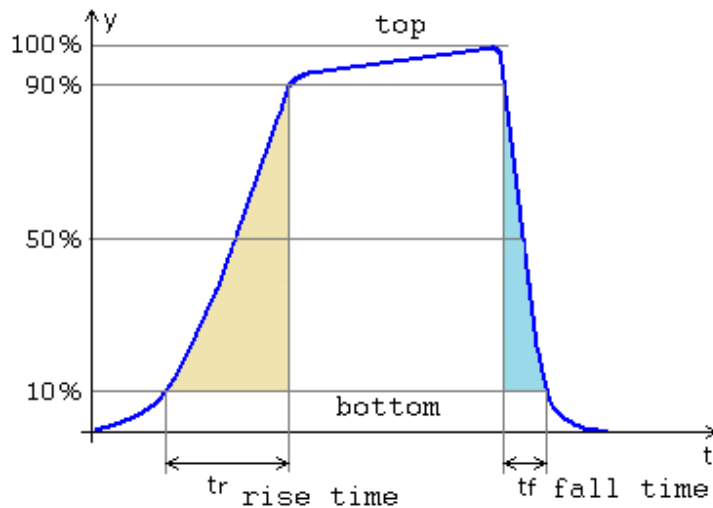
Figure 26 - Determining the rise time modified

source: (Mietke, 2019)

As for the Op amp the selection should consider the slew rate, a good unity-gain bandwidth and an appropriate voltage supply range. This corner requirements are satisfied with the LM7171, which is a high-speed voltage feedback amplifier for applications like pulse amplifiers and peak detectors. It is specified for +/- 5 V and +/- 15 V. The slew rate is defined as $4100 \frac{V}{\mu s}$ and the unity-gain bandwidth is defined as 200 MHz.

2.3.3.2.1   Slew rate

The slew rate is a very important property of an Op amp. It describes how fast the output of an Op amp can respond to a changing input. If this limit is exceeded, the output can be distorted and therefore prevents the input to be faithfully represented at the output.

In the case of the pulse generator the input current pulse is in the range of 20 to 30 ns. Measuring the generated pulse at the 50-Ohm resistance gives an overview on how fast the subsequent amplifier must be. In this specific application, the slew rate can be checked by calculating the voltage change within a nanosecond and comparing it with the slew rate. Since the output voltage step is proportional to the input current pulse, this comparison can be applied. It is only necessary to adjust the slew rate to the correct time (1 ns), since the slew rate is generally given in microseconds.

In Table 3, ten differential voltages were calculated for the output voltage step of the switched capacitance pulse generator. A time window of one nanosecond was applied. In general, it can be said that the OPamp is correctly selected when all differential voltages are below the slew rate of the OPamp. The slew rate for this time window is calculated as 4.1 V/ns.

Table 3 - Differential voltage per ns

Differential voltage within a nanosecond in V
0,6
1,28
2,16
1,56
0,32
0,76
0,98
0,68
0,12
0,04

2.3.3.2.2 Unity-gain bandwidth

The unity-gain bandwidth is the entire frequency range in which the amplifier can produce gain (Figure 27). (learningaboutelectronics, 2019)
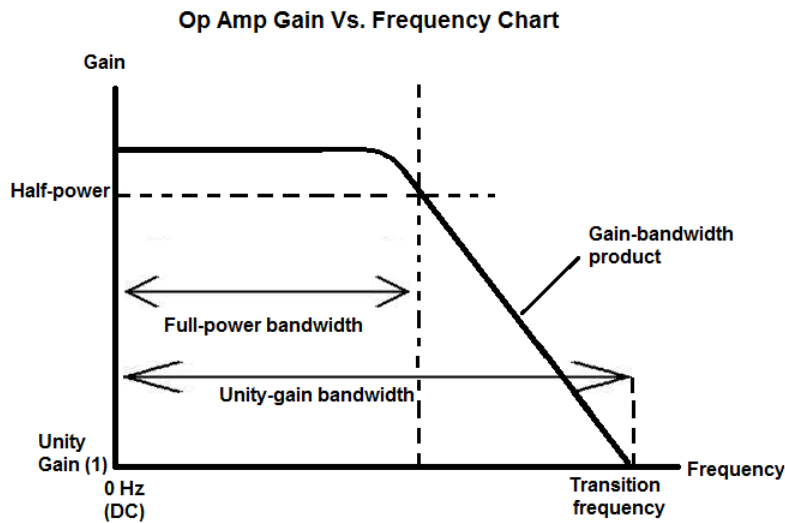
Figure 27 - Bode diagram of an OPamp in general

source: (learningaboutelectronics, 2019)

The transition frequency f_T determines the maximum frequency which the OP amp can produce gain. Above the f_T there is no gain, it is described as the cut-off point. Full-power bandwidth is guaranteed until reaching the cut-off frequency. At higher frequencies the gain is getting 20 dB/Dec weaker.

The frequency range of the pulse generator ranges from 1 kHz to 1 MHz as defined in the studies.

2.3.4 Comparator

2.3.4.1 Overview and Function

The comparator compares both input voltage levels and indicates if e.g. the voltage on the positive input is greater than the voltage level on the negative input. As a result, a high-level voltage signal is outputted. In the case of the opposite voltage level a low-level voltage signal is outputted. Usually a high-level voltage is within the range of the supply voltage but not above the maximum applied voltage level and a low voltage is often fixed at 0 V at the output. For the reference voltage a stable DC voltage was adjusted to serve as a threshold. Only the parts of the pulse which are above 50 % of the amplitude are registered during the measurement.

2.3.4.2 Comparator selection

Important properties of a comparator are the propagation delay, the supply voltage, the input voltage range as well as the output voltage levels. Additionally, the minimum registerable pulse width should not be undershot. A qualified comparator is the ADCMP600 with high speed instrumentation (3.5 ns propagation delay) and a small single supply (+2.5 V to +5.5 V) as well as an input voltage level range of -0.5 V to +5.8 V. The minimum pulse width is 4.5 ns at a single supply voltage of 5.5 V.

The propagation delay is the time to be reached to the point where the output reaches 50% of the output value. Therefore, this delay must be as short as possible to ensure that the counter gets the pulses delivered in time (ideally in real-time) and no information gets lost.

The minimum pulse width is another important parameter of the comparator to be considered. The input signal pulse should be above this value or as a consequence no signal will be outputted.

Lastly the "output voltage high level" must not undercut the "input voltage high level" of the counter. In this case a positive up-counting would not succeed if the voltage level is too low.

2.3.5 Counter

2.3.5.1 Overview and Function

For the counting part a 4-Bit binary counter was chosen due to its simplified usage and for its application in high-speed counting designs. It is commonly used as a frequency divider.

2.3.5.2 Counter selection

Two selection criteria are to be considered for the input voltage of high and low levels and the minimum pulse duration for the input signal to be correctly recognized. This criterion is fulfilled with the SN74LV161A 4-Bit synchronous binary counter. For minimum high-level state threshold is set to 3.5 V at the supply voltage of 5.5 V. The input voltage ranges from - 0.5 V to 7 V. The minimum pulse width is 5 ns. Additionally, the binary counter has a ripple-carry output, which produces a high-level pulse each time when the maximum of the counter is reached.

2.3.5.3 Counter configuration

FUNCTION TABLE

INPUTS					OUTPUTS				FUNCTION
$\overline{CLR}$	$\overline{LOAD}$	ENP	ENT	CLK	QA	QB	QC	QD	
L	X	X	X	X	L	L	L	L	Reset to "0"
H	L	X	X	↑	A	B	C	D	Preset Data
H	H	X	L	↑	No Change				No Count
H	H	L	X	↑	No Change				No Count
H	H	H	H	↑	Count up				Count
H	X	X	X	↑	No Change				No Count

Figure 28 - Function table of SN74LV161A

source: Datasheet SN74LV161A

In case that the binary counter is counting upwards, the inputs as above pictured (Figure 28) must be set high and the clock has to be provided with an input signal. In this case the input signal is the output signal of the comparator, which is either high (pulse peak detected) or low (threshold not exceeded). To grant no disturbances nor failed counts, all signal inputs (A, B, C and D) are set to ground. It ensures that the inputs are not accidentally set to a high level. This process was repeated for all other inputs and outputs which are not in use. The configuration "Count" was selected by applying a HIGH signal on CLR, LOAD, ENP, ENT and CLK.

3 Results

3.1 Pulse Generator

3.1.1 Simulation before setup

Some simulations regarding the selection of the transistor as well as the functionality of the researched circuit from the websites of (Wong, 2019) and (Engdahl, 2019) were made with the software LTSpice XVII. At first some simulation experiments with a standard 2N3904 bipolar transistor and with the Avalanche transistor ZTX415 were simulated.

A "Spice-model" of both transistors can be found in the web. This "Spice-model" tries to get as close as possible to the real transistor with the help of many parameters. Unfortunately, the available Spice-models from the web did not satisfy expectations about the Avalanche effect. It needs additional circuitry and for this reason further attempts discontinued.

The next step was to build a prototype or at least an experimental circuit on a breadboard with the standard Avalanche circuit without an external signal generator.

3.1.2 Measurement setup

The measurement setup contains a high voltage supply with adjustable current limitation and a standard oscilloscope to measure the output signal, see Figure 29.
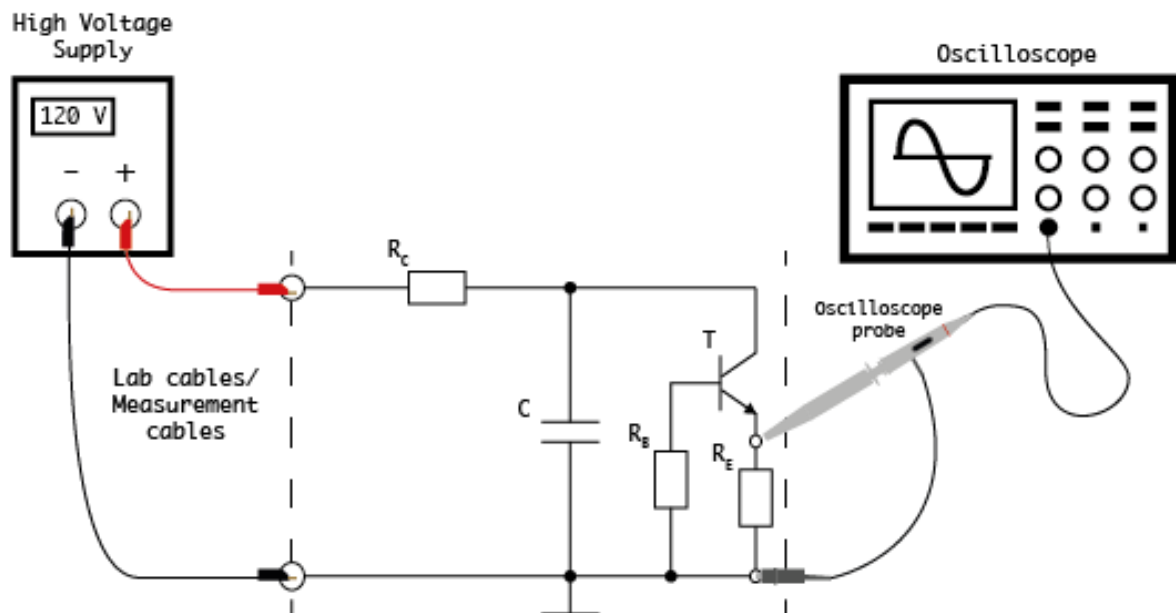
Figure 29 - Measurement setup for the standard Avalanche circuit
(without external signal generator)
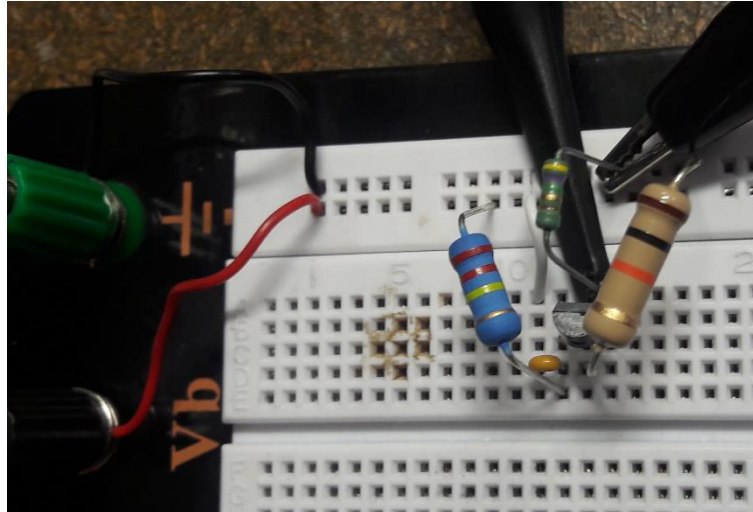
Figure 30 - Testing 2N3904 bipolar transistor on breadboard

During the measurement of the 2N3904 on the breadboard it was obvious, that influences from the parasitic connection points or wires act like antennas. Even inadvertent movements of the components would affect the signal shape. Therefore, the next step was to solder the components onto a stripboard with shorter wires and better-connected components. One important consideration was to solder banana jacks to the board in behalf of reduced noise and a stable connection to the high voltage source.

Figure 31 - Testing 2N3904 bipolar transistor soldered on a stripboard

After the successful operation of the avalanche pulse generator, the next step was to connect it to the CSP. After a few attempts, no output signal was obtained. The voltage supply of the operational amplifier, which should normally supply 5 V, dropped in some cases under 3 V. Due to these supply problems, further tests with the CSP were discontinued. For the further measurements the output voltage at the emitter resistor was used. This was not a problem, because the following components in the circuit require a voltage as an input variable.

3.1.3 Avalanche pulse analysis

3.1.3.1 Plug-in Version Testing (on breadboard)

In the first attempts the Avalanche trigger voltage was determined (see Figure 29 for test setup). At about 120 V the Avalanche effect occurred and the current pulse appeared at its maximum. For measuring reasons, the signal was measured at the 47 Ohm resistance as depicted in Figure 15, which occurred then as a proportional voltage pulse. The first results are based on the circuit of Version 1, as shown and explained in *2.3.1.1.*
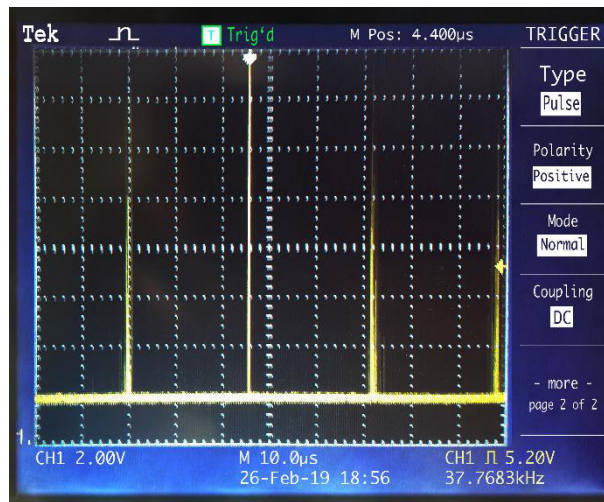
Figure 32- Testing 2N3904 - Avalanche effect – Multiple pulses - Circuit Version 1

In Figure 32 one can see the voltage peaks (> 15 V) produced by the Avalanche effect. In this measurement the transistor 2N3904 was tested on the breadboard. The pulse rate is about 37 kHz. The resisitance-capacitance combination is 220 kOhm and 100 pF.
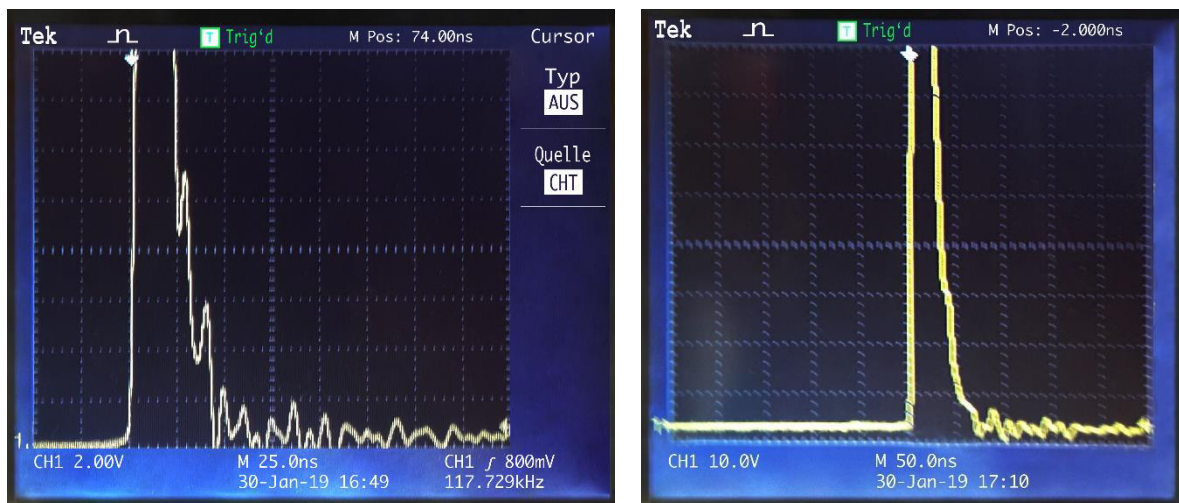
Figure 33 - Testing 2N3904 - Avalanche effect - pulse shape - Circuit Version 1
left picture: single pulse with 25 ns/div right picture: single pulse with 50 ns/div

Further testing with a different capacitance of 47 pF but with the same resistance of 220 kOhm reveals a pulse duration in the range of 30 to 40 ns. The pulse shape is also corrupted by noisy signal components. These interfering signal parts come from the oscilloscope probe to the circuit due to inferior connection. Additional interference components can be introduced into the signal if external forces act on the cable (for example, when lifting or pushing the cable). Interference can be minimized by placing the circuit on a printed circuit board and using proper connectors (Figure 33).

3.1.3.2   Soldered Version Testing (on stripboard)

Retesting the soldered version 2N3904 transistor on the stripboard shows lesser noise than before. After some tests with different capacitors, the decision was made for a 10-pF capacitor. The pulse length as well as the amplitude of the Avalanche signal is lower compared to larger capacitors. Therefore, the total amplitude is about 17.5 V and the pulse width is in the range of 30 ns.
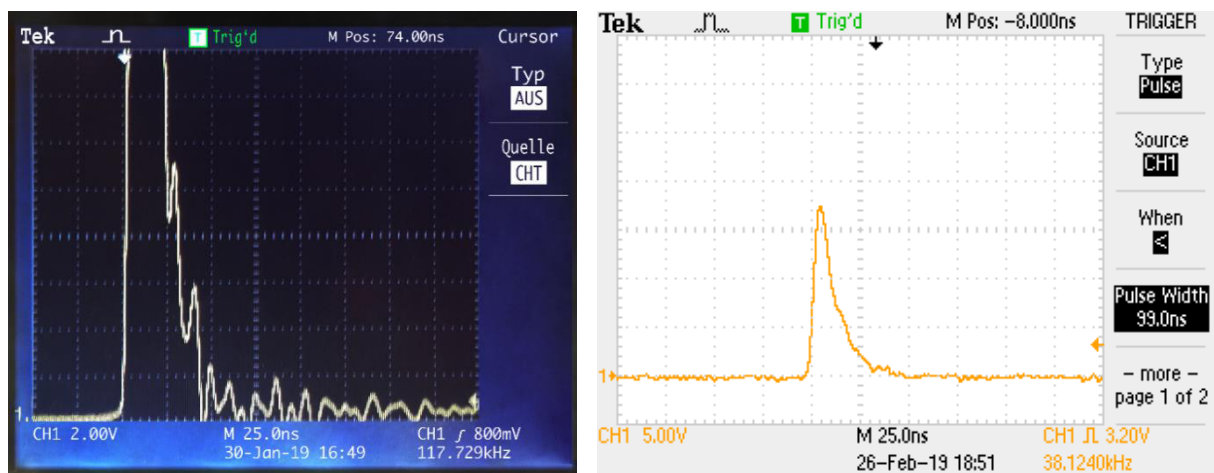
Figure 34 - Avalanche single pulse - comparison between plug-in (left) and soldered (right) Versions

If you now compare the soldered version with the plug-in version, one can see that the interference has been significantly minimized and a PCB version can provide further improvements in interference signal reduction.

The next step was to design the PCB with all circuit parts including the pulse generator, the CSP and the counting part. The same transistor was used, only its package changed to a SOT-23 mounting (MMBT3904). By repeating the tests as shown before, the maximum amplitude could be reduced and the pulse width stayed as before (Figure 36).

3.1.3.3 Testing an "Avalanche Transistor"
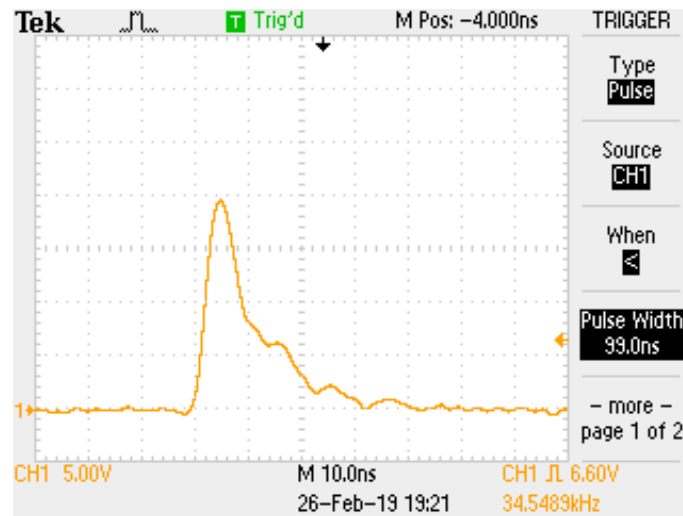
Figure 35 - Testing ZTX415 Avalanche transistor - pulse shape - Circuit Version 1

For experimental proposes another transistor was tested: ZTX415. Its datasheet claims that the ZTX415 is a special transistor designed for the Avalanche mode. As shown in Figure 35, the ZTX415 has a higher amplitude compared to the 2N3904. However, it has the same pulse width, which ranges from 30 ns to 40 ns (Figure 35). For further testing the ZTX415 did not have any other aspects to compete with the 2N3904. Even its Avalanche trigger voltage was about 320 V, which was a security issue. For these reasons, no further tests were made with the ZTX415.

3.1.3.4   Calculation of the total charge
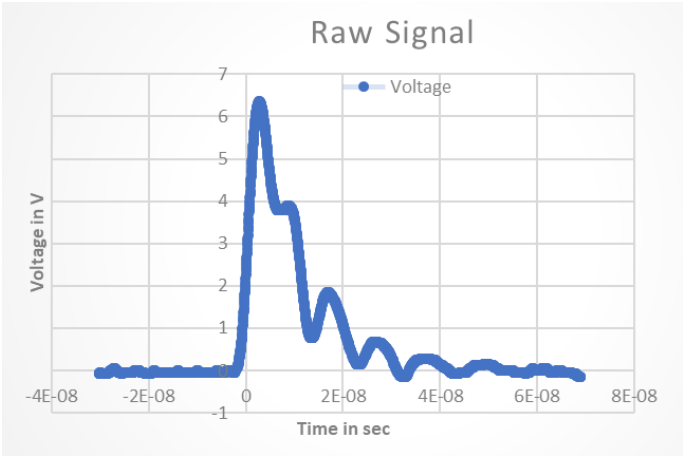
Figure 36 - Testing MMBT3904 on PCB - Avalanche pulse signal raw

For an exact examination of the signal property, the raw signal was cut in the time domain where the important signal parts are. The meaningful parts begin where the pulse starts at zero voltage and ends equally (Figure 37). In addition, the offset component was also subtracted from the original signal. For calculating the total charge one step is to determine the mean value of the voltage signal and eventually divide it by the resistance of 47 Ohm to get the mean current pulse signal.
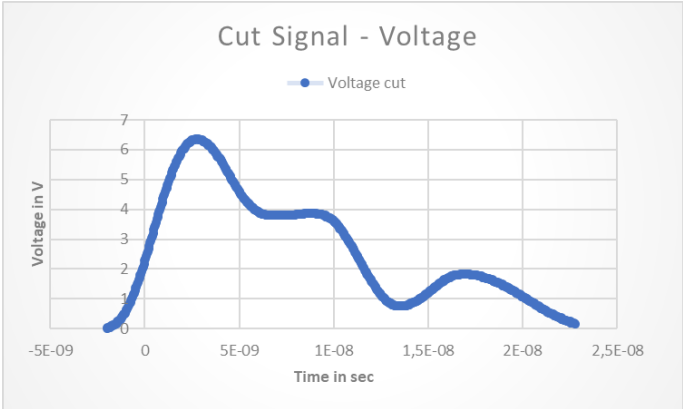
Figure 37 - Testing MMBT3904 on PCB - Avalanche pulse cut - Circuit Version 1
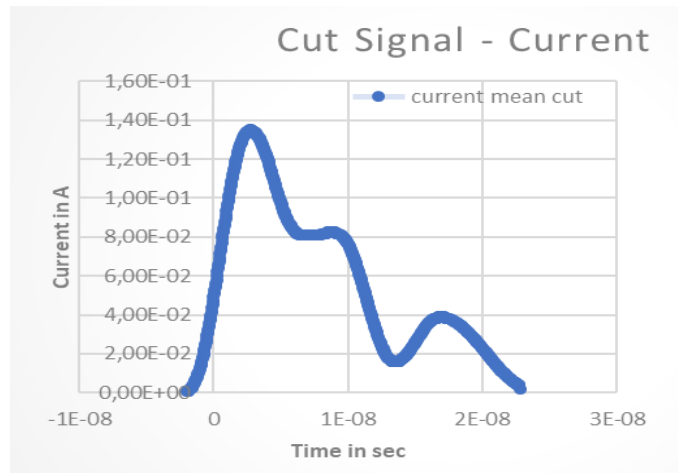
Figure 38 - Testing MMBT3904 on PCB - Avalanche Current pulse cut - Circuit Version 1

Following formula, as explained in the last chapter, has to be called in to calculate the total charge:

$$Q(t) = \int_0^t i(t)\,d\tau \qquad (4)$$

In case of the existing measurement results, the formula above has to be adjusted due to the discrete and finite values of the measurements.

$$Q = \frac{1}{R}\sum_0^m \bar{v}_m \cdot \Delta t \qquad (5)$$

Table 4 - Results MMBT3904 on PCB

Pulse duration	24.8 ns
Maximum voltage peak	6.36 V
Total charge	1.38 nC

The calculated total charge is in the range of 10^{-9} Farad (nano-range). The initially defined range of 10^{-15} farad (femto-range) was thus not achieved. Therefore, an attenuation is needed to lower the charge by an additional circuit.

3.1.4 External Pulse Triggering vs. Standard Avalanche Triggering
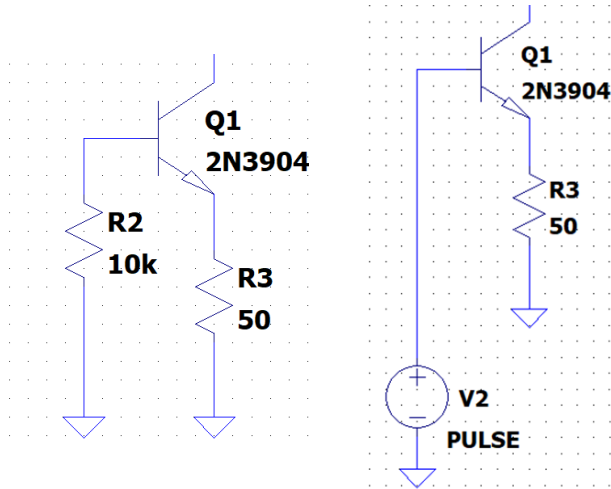
Figure 39 - External Triggering Source vs. Standard connection with resistance

As explained earlier, the difference between these two triggering procedures is the connection for the base at the transistor (Figure 39). The version with the resistance serves to complete the common-collector configuration (see section 2.2.4). In this case the Avalanche triggers at a much higher voltage (approximately 120 V) and the behaviour of pulse appearance can be described stochastically. On average a frequency of approximately 37 kHz can be measured. There is no possibility to change the frequency, because it is a component dependent phenomenon.
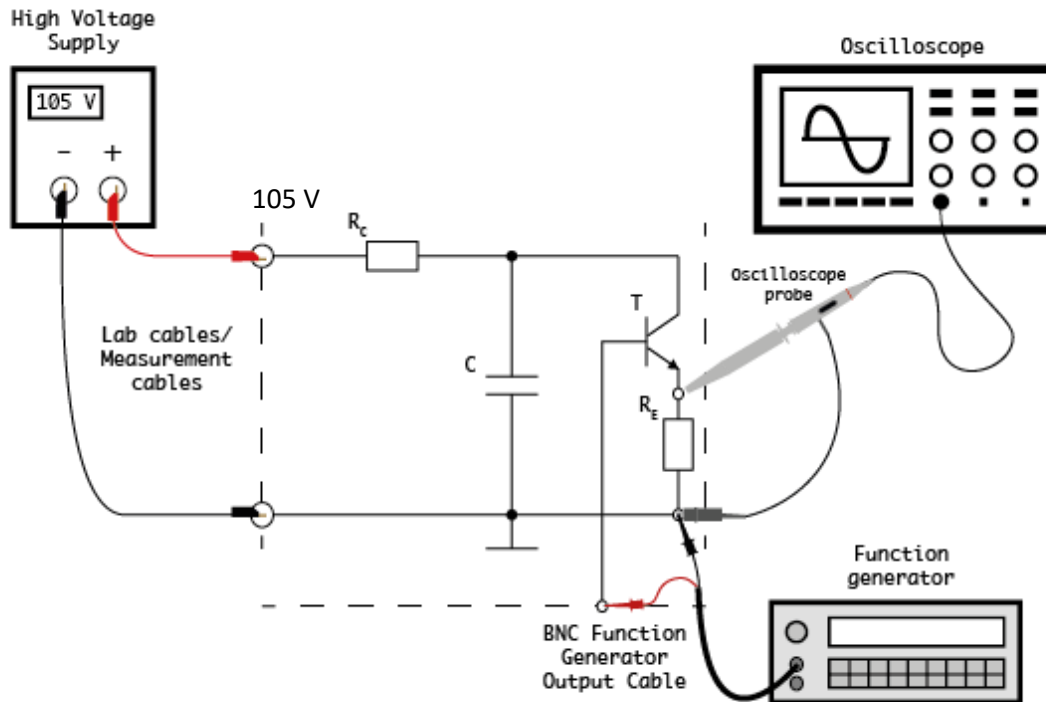
Figure 40 - Measurement setup for modified Avalanche circuit

The circuit from version 1 is now extended by an external pulse trigger. This is done with a function generator, which is connected to the base of the transistor. By provoking an external pulse trigger, the Avalanche occurs at approximately 105 V and the frequency is adjustable. The Avalanche pulse appears exactly at the beginning of each pulse (edge-triggered). The amplitude of the external pulse should not be very high, since it would disturb the correct comparison of the comparator with its threshold. The comparator threshold is also used to supress the external pulse. In further experiments only the external triggered version was used.
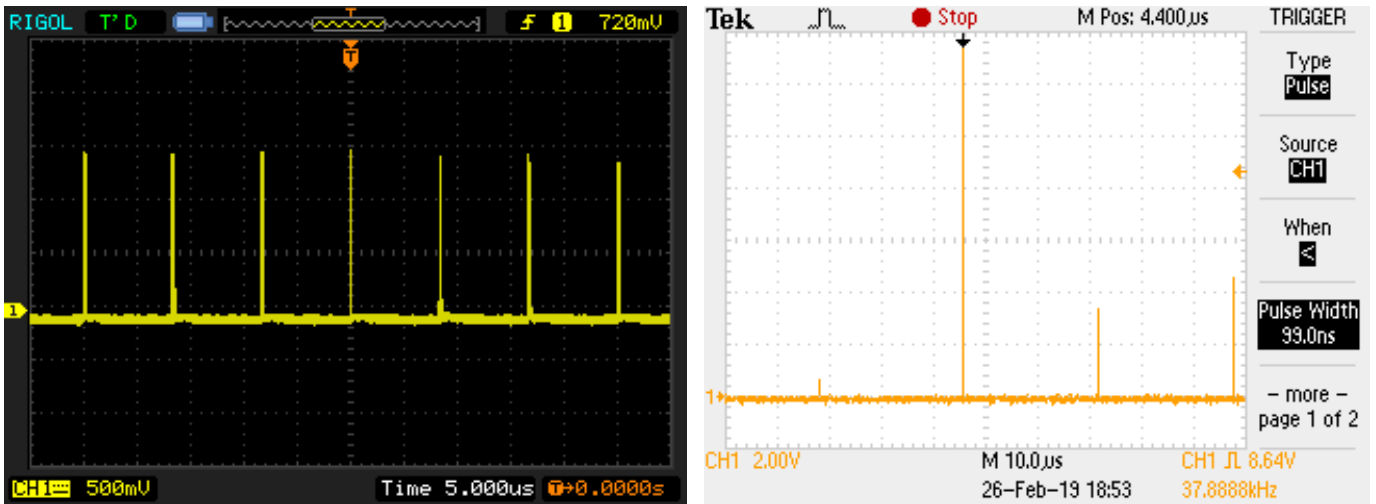
Figure 41 - Avalanche multiple pulses - Comparison between external triggered (left) and no triggering (right) Version

With the external pulse generator, it is now possible to generate evenly sized pulses, where the pulse rate can be additionally adjusted. In contrast to the non-triggered version, where the frequency cannot be changed and the pulses are different in amplitude (Figure 41).

3.1.5   Attenuation

An attenuator is a complex system that turned out to be difficult to design and build. We decided not to buy one, because good attenuators are very expensive and this work should remain within a reasonable financial framework. Therefore, the Institute for Electronics provided one of their 10dB-step attenuators. The following results were measured with the provided attenuator:
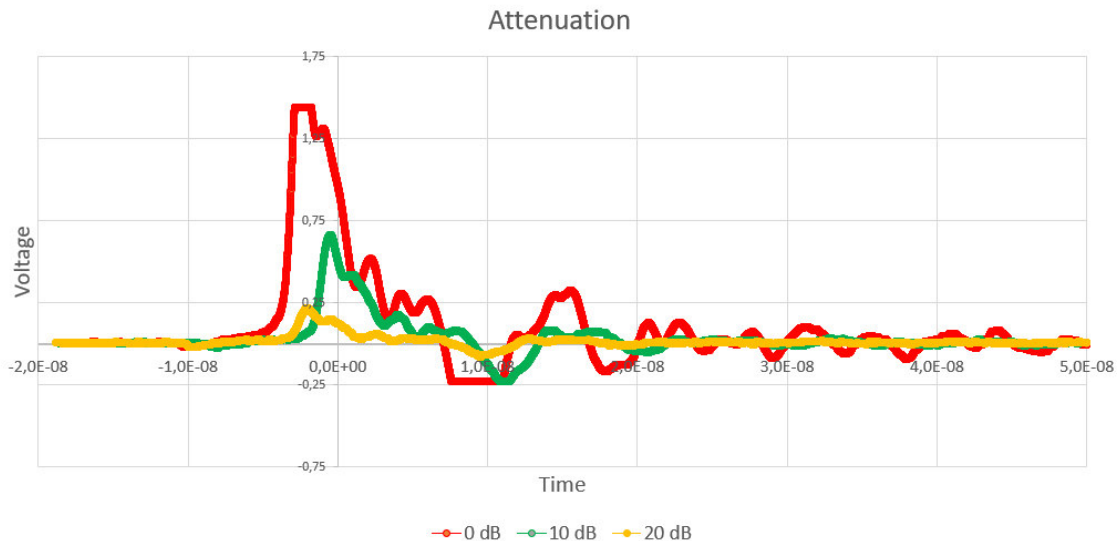
*Figure 42 - Comparing attenuation from: **0 dB** to **20 dB***

Table 5 - Attenuation maximum voltage peak

Attenuation	Voltage peak
0 dB	1.44 V
10 dB	0.66 V
20 dB	0.22 V

By connecting the attenuator to the pulse generator circuit part, the signal got attenuated to 1.52 V_{pp} and in further adjustments at 10 dB and 20 dB the amplitude sank as expected. Starting at 30 dB the signal was too small in the amplitude to be measured properly due to signal disturbances of the environment. In this example, the voltage at the output of the attenuator was measured in order to visualize the influence on the pulse signal in a simple way. Current and charge were not measured or calculated.

3.1.6 Avalanche Pulse evaluation

An important point when testing the avalanche pulse was whether its charge remained the same during repeated measurements. For this experiment three transistors with different breakdown voltages were chosen as well as different collector-emitter capacitances. 25 pulses were recorded for each transistor with the same resistances (220k Ohm, 50 Ohm) and capacitance (10 pF) for a plausible comparison. All experiments were measured with the external trigger pulse circuit (Version 2).

Table 6 - Transistors for pulse and charge evaluation (external pulse triggered Version)

Model name	Breakdown voltage	Avalanche appearance	Collector-Basis capacitance	Mean charge	Standard deviation charge
MMBT3904	60 V	105 V	4 pF	1,11 nC	3,59 pC
MMBT5550	140 V	346 V	30 pF	3,79 nC	5,57 pC
BFR92P	15 V	50 V	0.38 pF	330 pC	1,68 pC

As expected, all three transistors have different charges, as shown in Table 6. The lowest charge features the BFR92P. As for the evaluation for each transistor, the standard deviation for all transistors is in the pC - range, which indicates that the Avalanche pulse charge for each transistor is consistent due to the narrow distribution.

The most reliable charge consistency illustrates the MMBT5550 with a small standard deviation. It indicates that the measured data points tend to be close to the mean charge value.

3.1.7 Output signal analysis: Comparator and Counter
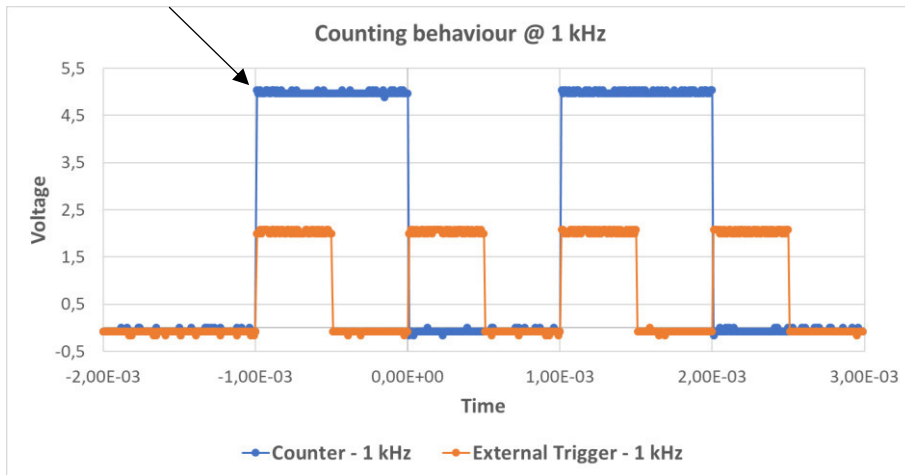
Figure 43 - Output signal Comparator and Counter
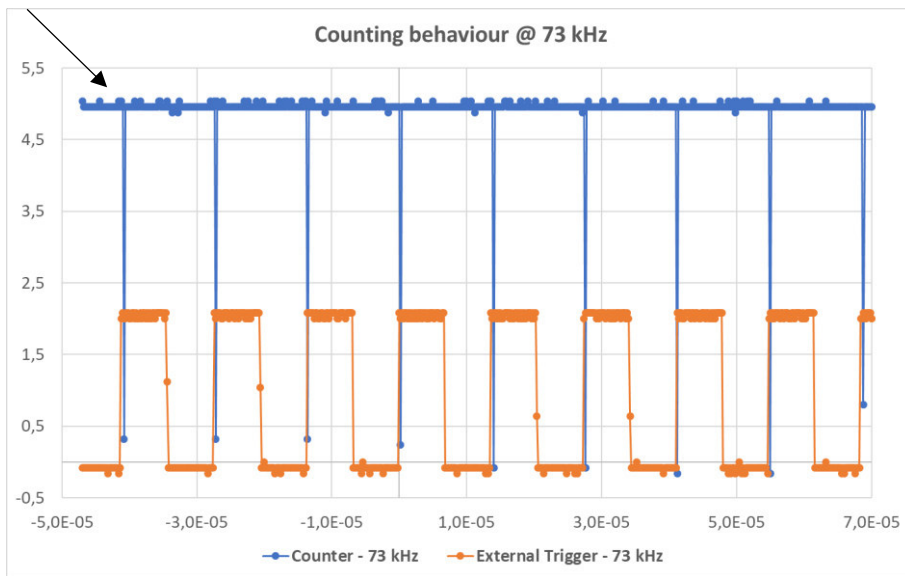
Figure 44 - Output signal Counter - Counting failure

The last measurement comprised the verification of the actual counting. Does the external triggered amount of pulses equal the output pulses registered by the counter?

In this case the counter acts secondarily as a frequency divider as mentioned in section 2.3.5. It suffices when the output pulse amount of the counter is multiplied by 2. Another phenomenon which emerges at higher frequencies can be seen in Figure 44. The Avalanche output signal of the pulse generator has slowly been attenuated. This reduces the pulse width so much that the rectangular shape can no longer be recognized. In other words, the duty cycle drops below 10%. Therefore, the comparator and its threshold can register the Avalanche pulse correctly and as a consequence the counter does not get the right signal on its input (Figure 45). The weakening of the Avalanche begins at 73 kHz and gets

worse with higher frequency until no signal can be observed. A mentionable point is the non-triggering under 1 kHz of the Avalanche effect.
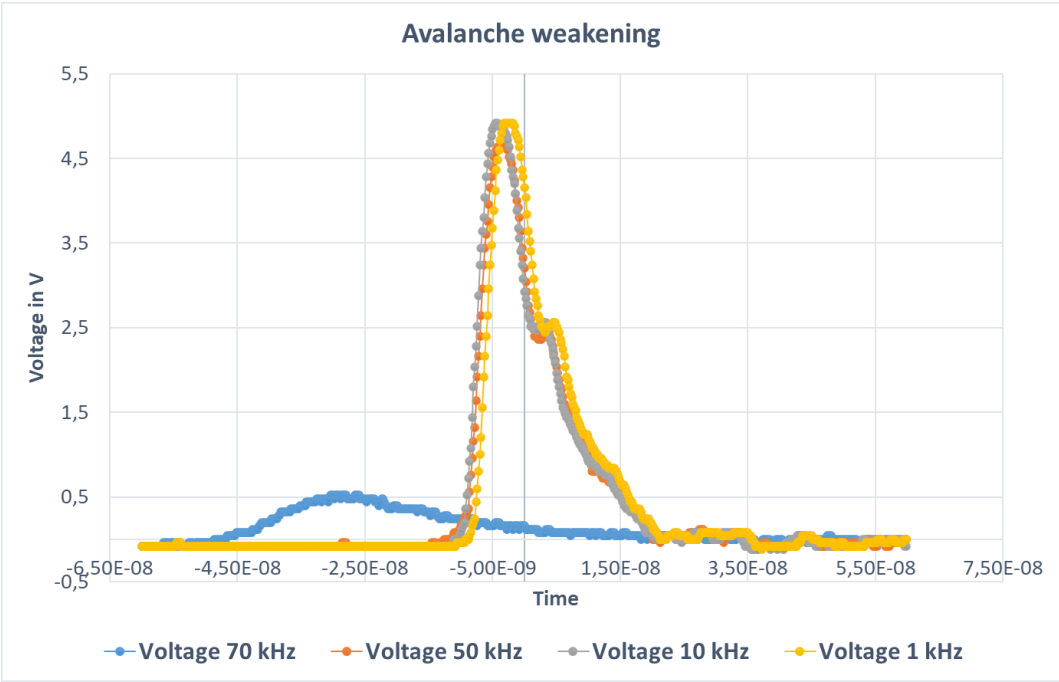
Figure 45 - Avalanche weakening in higher frequency

The final PCB can be seen in Figure 46. It contains the Avalanche pulse generator, the comparator part and the counting part with the connector pins for the NI USB 6501. To avoid second order effects, the final PCB had to be split in two parts. The other PCB consists of the secondary pulse generator "Switched capacitance" and two CSPs. The second PCB will be explained in the next section.
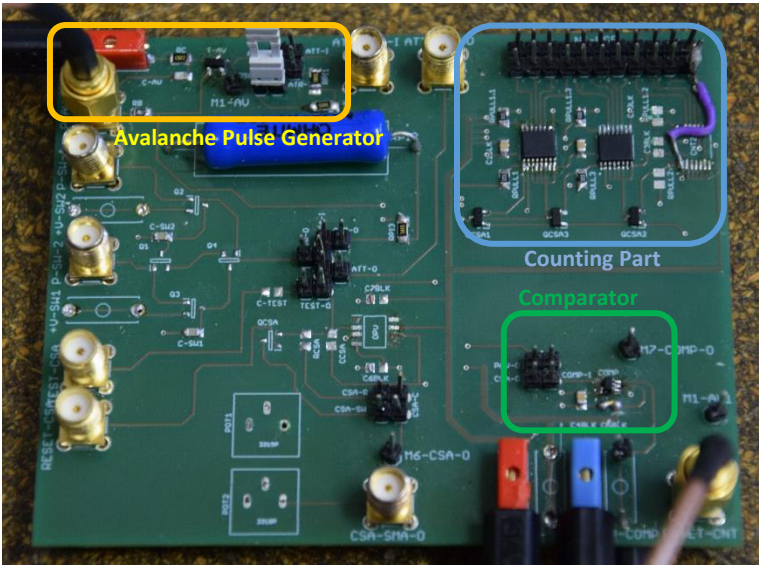
Figure 46 – Final Version of PCB: Avalanche pulse generator / Counting Part

3.2   Switched Capacitance Pulse Generator
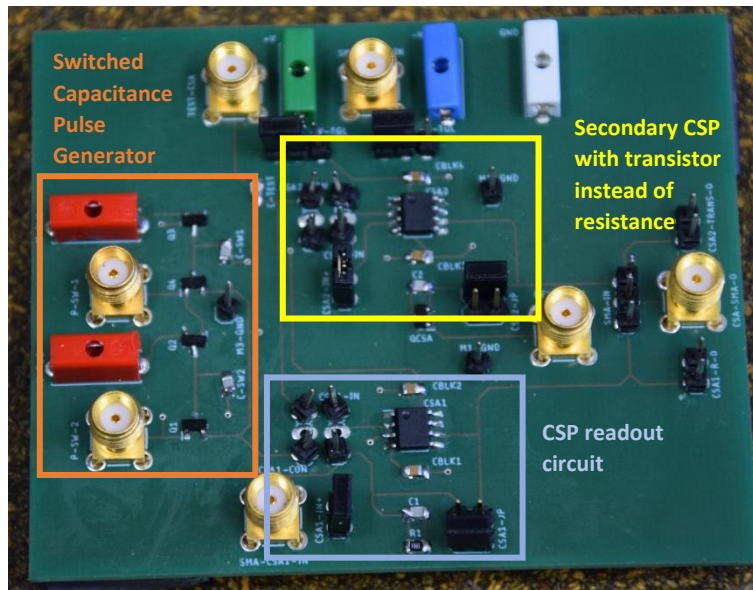
Figure 47 - Switched Capacitance PCB with CSP part

Two CSPs were built to test if there are any differences between controlled capacitance reset by using a transistor and a standard resistance in feedback. After some tests the CSP with the transistor could not achieve the same signal quality as the CSP with only the resistance. Due to some switching artefacts of the transistors the output signal was disturbed. Therefore, only the CSP with the resistance was used for further tests for the switched capacitance pulse generator.

3.2.1   Switched Capacitance pulse analysis

To determine the pulse width, the output voltage signal had to be measured in the rise time. The cursors had to be placed at 10% of the measured absolute pulse bottom and at 90 % of the measured absolute pulse top. A pulse width of 28.4 ns was measured. This method is explained in 2.3.1.2.

Figure 48 - Switched Capacitance - pulse width determination
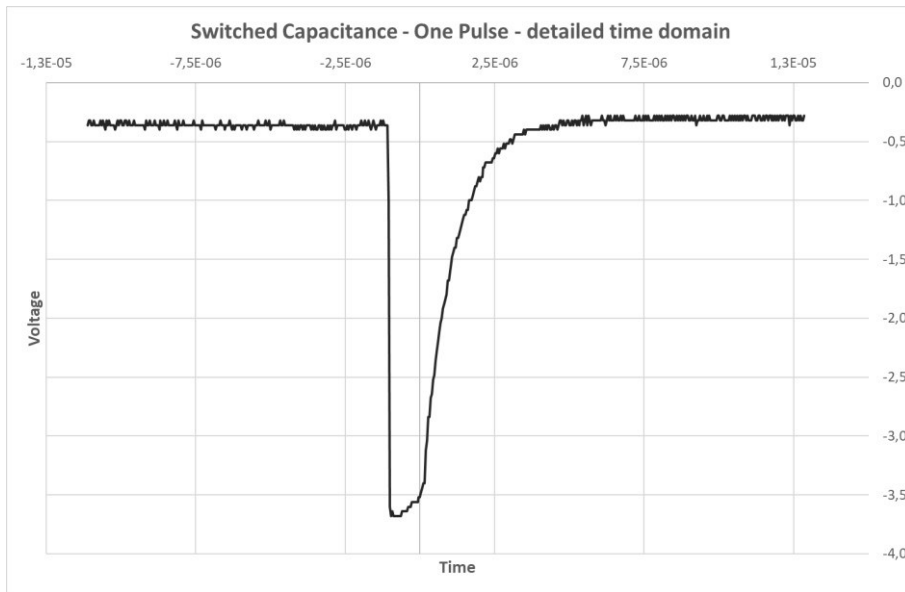
Figure 49 - Switched Capacitance - Output Voltage Signal CSP - detailed time domain

In Figure 49 one output voltage pulse of the CSP in detailed view in the time domain can be seen. The output voltage is negative due to the phase shift behaviour of the integrator circuit (OP amp). In the next Figure 50 a multi-pulse view of the CSP output is displayed. It is also clearly seen that the placement of the external pulses in the time domain for the toggling of the transistors is not perfectly met. The distance between each peak pair is irregular.
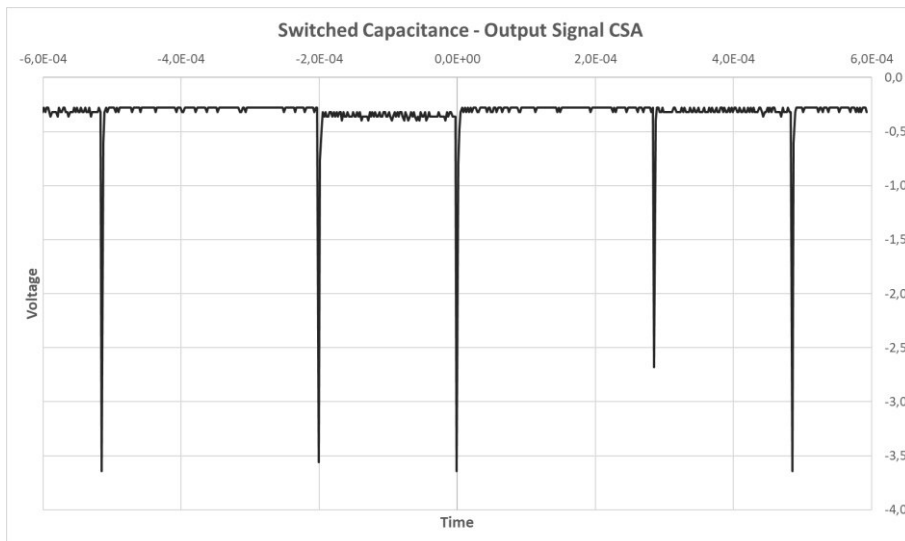
Figure 50 - Switched Capacitance - Output Signal CSP – Standard

3.2.2 Switched Capacitance Pulse evaluation

The pulse evaluation was repeated exactly as for the Avalanche pulse with 25 pulses. The total charge was calculated for each pulse. The number of charges in a specific range were then plotted in a bar chart again. The bar chart visualizes the distribution of the number of pulses in a specific charge range. Due to the small charge range the total charge can be considered as stable.

Table 7 - Pulse evaluation - Switched Capacitance

Charge mean	4,82 nC
Charge standard deviation	0,165 pC
Maximum amplitude	3,68 V

The SC standard deviation is very small and therefore indicates an excellent consistency of the overall charge.

3.3 Comparison with another Avalanche Pulse Generator

3.3.1 Overview

Finally, a comparison with another avalanche pulse generator is made. This is an avalanche transistor-based nanosecond pulse generator from the Institute for Experimental Quantum Metrology from the Physikalisch-Technische Bundesanstalt, Braunschweig, Germany (Nikolai Beev, 2017).

The team of the Physikalisch-Technische Bundesanstalt developed an avalanche pulse generator to drive a photocathode of an image intensifier. Its pulse generator consists of multiple avalanche transistors connected in parallel as well as connected together at the output. These transistors are triggered sequentially and have the same load. In Figure 51 you can see the circuit that was used in their work. One used the same principle as this thesis to trigger the avalanche with an external trigger source at the base of the transistor. For the generation of the trigger pulses a so-called "Xilinx Spartan-3 FPGA" was used. The output pulses are set in the range of nanoseconds and the pulse rate is in the range of 25 MHz, whereas each single transistor achieve a maximum repetition rate of 4 MHz.
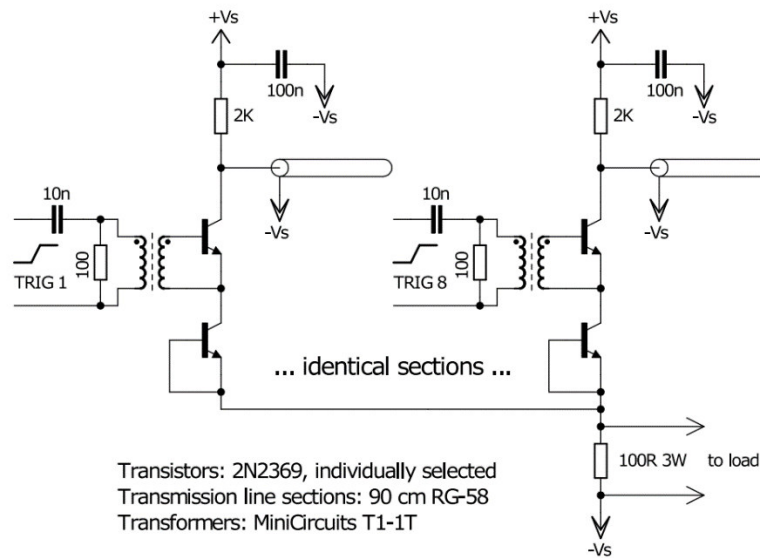
Figure 51 - Avalanche Pulse Generator from Institute of Experimental Quantum Metrology
source: (Nikolai Beev, 2017)

3.3.2 Comparison of the components

In the following table (Table 8) the relevant values for the avalanche pulse are compared. The 2N2369 NPN bipolar transistor of the Institute of E.Q.M. is compared to the bipolar transistor of this master thesis (2N3904 NPN).

As comparison values the break down voltage from the collector-emitter and the input and output capacitance were chosen. The values are almost identical, only the input capacity of the 2N2369 is 4 pF smaller.

Table 8 – Comparison between transistors

	Transistor model	Breakdown voltage Collector-Emitter	Capacitance input/output
Master Thesis	2N3904	40 V	8 pF / 4 pF
APG from Institute of E.Q.M.	2N2369	40 V	4 pF / 4 pF

Other comparative values cannot be used in this case because the focus in the work of the Institute of E.Q.M. was different. The values of the capacitor and the resistor were not published in this work.

The work of the E.Q.M. gives information about the choice of the transistor. The comparison shows that the breakdown voltage as well as the input and output capacitances have been well chosen for an avalanche pulse generator.

4 Discussion

4.1 Avalanche Pulse signal analysis

4.1.1 Avalanche Pulse for Environmental Testing

Can an Avalanche Pulse Generator be used for testing a detector system? If the research information about PcCT is called to mind then the first important aspect for the testing environment is the pulse shape and charge consistency. Another point is that multiple photons can occur in different time spans. Each of this photon have individual amplitudes and their pulse width is described in nanosecond range.

The Avalanche pulse is consistent in shape and in total charge as one can see in the results section. However, the falling edge of the Avalanche pulse has multiple signal bumps, which can be traced back to a not perfectly matched wave impedance. Therefore, signal reflections occur and alter the output signal. The next mentionable point is the pulse rate. It is limited to a maximum frequency of 73 kHz, where the Avalanche pulse suddenly becomes weaker in amplitude. Lastly, the pulse width is at least in the nanosecond range but exceeds the 20-nanosecond suggested range from the literature studies.

Eventually the Avalanche Pulse Generator could be a potential candidate for a testing environment for PcCT detectors if the pulse shape as well as the frequency range were reasonably fitted to the real conditions of PcCT detectors. This means that the pulse rate should be adjustable up to the MHz range and that the pulse shape especially the falling edge should be falling steeper. The matching of the wave impedance may have also an influence on the overall pulse width.

The amplitude could be better attenuated if using other technical solutions such as the mentioned circuits for attenuation (T-Pad and current divider).

4.1.2 Comparison between Avalanche and Switched Capacitance - Pulse Generation

Table 9 - Comparison between Avalanche and Switched Capacitance

Pulse Generator	Avalanche	Switched Capacitance
Pulse width	24.8 ns	28.4 ns
Total charge	1.38 nC	4.82 nC

The Switched Capacitance circuit is set up to have a comparison with the Avalanche Pulse Generator. Both circuits have shown that they have good total charge stability and the ability to adjust the pulse rate and amplitude. However, the pulse rate of the Switched capacitance has a wider frequency range than the Avalanche pulse rate. It was tested up to 1 MHz. Neither the Avalanche nor the Switched Capacitance could get down to the femto-Coulomb-range. Both mean charges were in the nano-Coulomb-range. The Switched capacitance pulse width was slightly longer than the pulse width of the Avalanche circuit.

4.2 Future Outlook

The Avalanche Pulse Generator has some major issues if using it as a testing environment for PCD. Primary the pulse shape as well as the pulse rate must be adjusted first. Some additional experiments regarding the circuit components (resistance and capacitance) could give answer to the limitation of the pulse rate. Testing different transistors (breakdown voltage and Collector-Emitter capacitance) could give more information about the behaviour of the Avalanche effect itself in size and duration of the pulse. Another point to consider when designing both pulse generators is the scaling down of the transistor size. This not only affects the dimensions, but also the electrical properties such as parasitic capacitance or current. Lastly the total charge could be downsized better additional circuitry as shown with the T-Pad or the current divider. (Fikru Adamu-Lema, 2020)

4.3 Conclusion

The Avalanche effect is an interesting aspect of a transistor and can be used for generating very short pulses. Understanding on how the Avalanche effect works and how to manipulate it properly to achieve the desired results is essential. Using the Avalanche effect for a testing environment for PCD is possible and can give pulses in the ns-range. By adding additional circuitry e.g. current divider, the amplitude can be adjusted and therefore different energy levels can be generated.

5 Bibliography

Abdulla, S. (2019, 10 30). *radiologycafe*. Retrieved from radiologycafe:
    https://www.radiologycafe.com/radiology-trainees/frcr-physics-notes/spect-imaging

Academy, K. (Director). (2019). *PN breakdown and avalanche* [Motion Picture].

Advacam. (2019, 11 18). *Advacam - Youtube*. Retrieved from Advacam - Youtube:
    https://www.youtube.com/watch?v=yyi96FBeGb8

Alberto Pullia, F. Z. (2010). *Automatic Offset Cancellation and Time-ConstantReduction in Charge-Sensitive Preamplifiers.* IEEE TRANSACTIONS ON NUCLEAR SCIENCE.

Ari Kilpela, J. K. (1997). *Laser pulser for a time-of-flight laser radar.* American Institute of Physics.

Arizona Institute of Urology. (2019, 10 30). *aiurology*. Retrieved from aiurology:
    https://www.aiurology.com/diagnostic-ct-scan-center.html

Aspencore. (2019, 10 30). *electronics-tutorials*. Retrieved from electronics-tutorials:
    https://www.electronics-tutorials.ws/transistor/tran_1.html

Brall, F. (30. 10 2019). *rn-wissen*. Von rn-wissen: https://rn-wissen.de/wiki/index.php/Abblockkondensator abgerufen

C.G. Jakobson, G. A. (1999). *Low noise CMOS readout for CdZnTe detector arrays.* Elsevier.

Cervantes, G. A. (2016). Digital radiography. In G. A. Cervantes, *Technical Fundamentals of Radiology and CT* (pp. 24-1 to 24-13). IOP Publishing.

Cheever, E. (2019, 11 19). *swarthmore.edu*. Retrieved from swarthmore.edu - SwitchedCap:
    http://www.swarthmore.edu/NatSci/echeeve1/Ref/FilterBkgrnd/SwitchedCap.html

Circuitglobe. (2019, 10 30). *Circuitglobe*. Retrieved from Circuitglobe: https://circuitglobe.com/jk-flip-flop.html

Cremat. (2019, 10 30). *cremat*. Retrieved from cremat: http://www.cremat.com/why-use-csps/

Cuttone, G., Marchetta, C., Torrisi, L., Mea, G. D., Quaranta, A., Rigato, V., & Zandolin, S. (1997). *Surface treatment of HV electrodes for superconducting cyclotron beam extraction.* IEEE. Retrieved from G. Cuttone, C. Marchetta, L. Torrisi, G. Della Mea, A. Quaranta, V. Rigato and S. Zandolin, Surface Treatment of HV Electrodes for Superconducting Cyclotron Beam Extraction,

Dössel, O. (2016). *Bildgebende Verfahren in der Medizin* (2 Ausg.). Heidelberg, Berlin: Springer-Verlag.

Elprocus. (2020, 1 28). *Elprocus*. Retrieved from https://www.elprocus.com/avalanche-transistor-circuit-working-characteristics/

Engdahl, T. (2019, 10 30). *epanorama*. Retrieved from epanorama:
    http://www.epanorama.net/newepa/2016/11/17/avalanche-pulse-generator-circuit/

Fikru Adamu-Lema, D. (2020, 4 19). *University of Glasgow.* Retrieved from Mirco to Nano:
    http://userweb.eng.gla.ac.uk/fikru.adamu-lema/

Huiming Zeng, T. W. (2013). *Design of a Low-Noise Front-End Readout CSP-Shaper.* Journal of Signal and Information Processing.

Jedec. (2019, 10 30). *Jedec*. Retrieved from Jedec: https://www.jedec.org/standards-documents/dictionary/terms/breakdown-voltage-collector-emitter-base-open-vbrceo%c2%a0formerly%c2%a0b

Katsuyuki Taguchi, J. S. (2013). *Vision 20/20: Single photon counting x-ray detectors in medical imaging.* American Association of Physicists in Medicine.

Laube, P. (2019, 10 30). *halbleiter*. Retrieved from halbleiter: https://www.halbleiter.org/grundlagen/der-p-n-uebergang/

learningaboutelectronics. (2019, 10 30). *learningaboutelectronics*. Retrieved from learningaboutelectronics: http://www.learningaboutelectronics.com/Articles/Op-amp-unity-gain-bandwidth

Liqiang Ren, B. Z. (2017). *Tutorial on X-ray photon counting detector characterization.* IOS Press.

Lutz, G. (2007). *Semiconductor Radiation Detectors.* Heidelberg, Berlin: Springer-Verlag.

Martin J. Willemink, M. P. (2018). *Photon-counting CT: Technical Principles and Clinical Prospects.* RSNA.

Medical Imaging System Labs. (2019, 10 30). *Medical Imaging System Labs*. Retrieved from Medical Imaging System Labs: https://web.yonsei.ac.kr/msl/Research.htm

Medmovie. (2019, 10 30). *medmovie*. Retrieved from medmovie: https://medmovie.com/library_id/3090/topic/cvml_0223i/summary/

Meek, J. M., & Craggs, J. D. (1978). *Electrical Breakdown of Gases .* Chichester: John Wiley & Sons.

Mietke, D. (30. 10 2019). *Elektroniktutor*. Von Elektroniktutor: https://elektroniktutor.de/signalkunde/signdat.html abgerufen

National Instruments Forum. (2019, 10 30). Retrieved from National Instruments Forum: https://forums.ni.com/t5/LabVIEW/USB-6501-COUNTER/m-p/599022?profile.language=en&requireLogin=False

Nave, R. (2019, 10 30). *hyperphysics*. Retrieved from hyperphysics: http://hyperphysics.phy-astr.gsu.edu/hbase/Electronic/jkflipflop.html#c1s

Nikolai Beev, J. K. (2017). *Note: An avalanche transistor-based nanosecond pulse generator.* Bundesallee 100, 38116 Braunschweig, Germany: QUEST Institute for Experimental Quantum Metrology, Physikalisch-Technische Bundesanstalt.

physicsopenlab. (2019, 10 30). *physicsopenlab*. Retrieved from physicsopenlab: http://physicsopenlab.org/2017/09/27/charge-sensitive-preamplifier/

Picclick. (2020, 2 2). *Picclick*. Retrieved from Picclick: https://picclick.com/HP-8494A-Freq-Range-DC-4Ghz-11-dB-Attenuator-352392056473.html

Polad M. Shikhaliev, T. X. (2005). *Photon counting computed tomography: Concept and initial results.* Medical Physics Journal.

R. Ballabriga, J. A. (2016). *Review of hybrid pixel detector readout ASICs for spectroscopic X-ray imaging.* IOP, Sissa Medialab.

radiopaedia. (2019, 10 30). *radiopaedia*. Retrieved from radiopaedia: https://radiopaedia.org/cases/normal-abdominal-x-ray

ROHM Co., L. (2020, 4 13). *Tech Web*. Retrieved from What are MOSFETs? - MOSFET Parasitic Capacitance and Its Temperature Characteristic: https://techweb.rohm.com/knowledge/si/s-si/03-s-si/4873

ROHM Co., L. (2020, 5 11). *Techweb*. Retrieved from ROHM Co.,Ltd.: techweb.rohm.com/knowledge/si/s-si/03-s-si/4873

Shuai Leng, P. M. (2019). *Photon-counting Detector CT: System Design and Clinical Applications of an Emerging Technology.* Radiological Society of North America, Inc.

sprut. (30. 10 2019). *sprut*. Von sprut: http://www.sprut.de/electronic/switch/pkanal/pkanal.html abgerufen

Stiles, J. (2011). *BJT Internal Capacitances.* Kansas: The Univeristy of Kansas - Dept. of EECS.

Sze, S. M., & Ng, K. K. (2007). *Physics of Semiconductor Devices.* Hoboken, New Jersey: John Wiley & Sons.

W. Zhou, J. L. (2018). *Comparison of a Photon-Counting-Detector CT with an Energy-Integrating-Detector CT for Temporal Bone Imaging: A Cadaveric Study.* American Journal of Neuroradiology.

Whittemore, A. (2019, 10 30). *hackaday*. Retrieved from hackaday: https://hackaday.io/project/2226-avalanche

Wikipedia. (2019, 12 9). *Wikipedia*. Retrieved from Wikipedia: https://en.wikipedia.org/wiki/Current_divider

Wong, K. D. (2019, 10 30). *kerrywong*. Retrieved from kerrywong: http://www.kerrywong.com/2013/05/18/avalanche-pulse-generator-build-using-2n3904/

Yermie. (2019, 10 30). *memorangapp*. Retrieved from memorangapp: https://www.memorangapp.com/flashcards/29654/Specific+Therapeutic+Positions+and+Crutch+Walking+Gaits/

Zhenjie Li, Q. L. (2017). *Development of an integrated four-channel fast avalanche-photodiode.* Elsevier.

Zibo Li, P. S. (2019, 10 30). *semanticscholar*. Retrieved from semanticscholar: https://www.semanticscholar.org/paper/Radiopharmaceutical-chemistry-for-positron-emission-Li-Conti/f115bcf13a1eab819af72e0023333512bf6a31ff

5.1 List of Illustrations

5.2 List of tables

5.3   LIST OF FORMULAS

6 Appendix

- Eagle: Circuit Schematic Avalanche Part 1

- Eagle: PCB Schematic Avalanche

- Eagle: Circuit Schematic Switched Capacitance & CSP

- Eagle: PCB Schematic Switched Capacitance & CSP